The Electronic Structures of an Isostructural Series of Octahedral Nitrosyliron Complexes {Fe−NO}^{6,7,8} Elucidated by Mössbauer Spectroscopy

Christina Hauser, Thorsten Glaser, Eckhard Bill,* Thomas Weyhermüller, and Karl Wieghardt*

Contribution from the Max-Planck-Institut für Strahlenchemie, Stiftstrasse 34-36, D-45470 Mülheim a.d. Ruhr, Germany

Received November 29, 1999

Abstract: From the reaction of *cis*-[(cyclam)$Fe^{III}(Cl)_2$]Cl (cyclam = 1,4,8,11-tetraazacyclotetradecane) with hydroxylamine in water the octahedral nitrosyliron complexes *trans*-[(cyclam)Fe(NO)Cl](ClO_4) (**1**) and *cis*-[(cyclam)Fe(NO)I]I (**2**) have been isolated as crystalline solids. EPR spectroscopy and variable-temperature susceptibility measurements established that **1** possesses an $S = {}^1/_2$ and **2** an $S = {}^3/_2$ ground state; both species are of the {Fe−NO}^{7} type. Electrochemically, **1** can be reversibly one-electron oxidized yielding *trans*-[(cyclam)-Fe(NO)Cl]$^{2+}$, an {Fe−NO}^{6} species, and one-electron reduced yielding *trans*-[(cyclam)Fe(NO)Cl]^0, an {Fe−NO}^{8} species. These complexes have been characterized in CH_3CN solutions by UV−vis and EPR spectroscopy; both possess a singlet ground state. All of these nitrosyliron complexes, including [LFe(NO)$(N_3)_2$] ($S = {}^3/_2$; L = 1,4,7-trimethyl-1,4,7-triazacyclononane) and [L′Fe(NO)(ONO)(NO_2)](ClO_4) ($S = 0$; L′ = 1,4,7-triazacyclononane), have been studied by variable-temperature Mössbauer spectroscopy both in zero and applied fields. The oxidation of **1** is best described as metal-centered yielding a complex with an Fe^{IV} ($S = 1$) coupled antiferromagnetically to an NO^- ($S = 1$), whereas its reduction is ligand-centered and yields a species with a low-spin ferric ion ($S = {}^1/_2$) antiferromagnetically coupled to an NO^{2-} ($S = {}^1/_2$). In agreement with Solomon et al. (*J. Am. Chem. Soc.* **1995**, *117*, 715) both {Fe−NO}^{7} ($S = {}^3/_2$) species in this work are described as high-spin ferric ($S = {}^5/_2$) antiferromagnetically coupled to an NO^- ($S = 1$). Complex **1** is proposed to contain an intermediate spin ferric ion ($S = {}^3/_2$) antiferromagnetically coupled to NO^- ($S = 1$). The alternative descriptions as low-spin ferric antiferromagnetically coupled to NO^- ($S = 1$) or low-spin ferric with an NO^- ($S = 0$) ligand are ruled out by the applied field Mössbauer spectra.

Introduction

Non-heme ferrous centers in a number of metalloproteins are known to react reversibly with NO[1−7] with formation of paramagnetic nitrosyliron centers which according to the Enemark and Feltham notation[8] are of the {Fe−NO}^{7} type. These non-heme iron enzyme nitrosyl derivatives invariably possess an EPR-active $S = {}^3/_2$ ground state. In inorganic chemistry[9−11] two complexes have become archetype models, namely [Fe(EDTA)(NO)][1] and [LFe(NO)$(N_3)_2$],[11] where EDTA represents the dianion of ethylenediaminetetraacetic acid and L is 1,4,7-trimethyl-1,4,7-triazacyclononane. Both species are of the type {Fe−NO}^{7} ($S = {}^3/_2$) and the latter complex has been structurally characterized[11] and spectroscopically studied by using X-ray absorption,[12a,b] resonance Raman, magnetic circular dichroism, electron paramagnetic resonance,[12a] and, in part, Mössbauer spectroscopies as well as SQUID magnetic susceptibility.[12a] In addition, SCF-Xα-SW[12a] and, very recently, GGA[3] density functional calculations have been reported. Table 1 lists some spectroscopic properties of these model complexes and metalloproteins.

It is therefore rather discomforting that despite these enormous spectroscopic efforts and calculations using the most advanced computational programs available the conclusions with regard to the best description of the electronic structure of this important class of {Fe−NO}^{7} ($S = {}^3/_2$) complexes remains to be somewhat controversial.[3,12] While Solomon et al.[12] have presented compelling spectroscopic evidence (with the exception of Mössbauer

(1) Arciero, D. M.; Lipscomb, J. D.; Huynh, B. H.; Kent, T. A.; Münck, E. *J. Biol. Chem.* **1983**, *258*, 14981.
(2) Nocek, J. M.; Kurtz, D. M., Jr.; Sage, J. T.; Xia, Y.-M.; Debrunner, P.; Shiemke, A. K.; Sanders-Loehr, T. M. *Biochemistry* **1988**, *27*, 1014.
(3) Rodriguez, J. H.; Xia, Y.-M.; Debrunner, P. *J. Am. Chem. Soc.* **1999**, *121*, 7846.
(4) Bill, E.; Bernhardt, F.-H.; Trautwein, A. X.; Winkler, H. *Eur. J. Biochem.* **1985**, *147*, 177.
(5) Haskin, C. J.; Ravi, N.; Lynch, J. B.; Münck, E.; Que, L., Jr. *Biochemistry* **1995**, *34*, 11090.
(6) Chen, V. J.; Orville, A. M.; Harpel, M. R.; Frolik, C. A.; Sureros, K.; Münck, E.; Lipscomb, J. D. *J. Biol. Chem.* **1989**, *264*, 21677.
(7) Orville, A. M.; Chen, V. J.; Kriauciunas, A.; Harpel, M. R.; Fox, B. G.; Münck, E.; Lipscomb, J. D. *Biochemistry* **1992**, *31*, 4602.
(8) Enemark, J. H.; Feltham, R. D. *Coord. Chem. Rev.* **1974**, *13*, 339. (b) Feltham, R. D.; Enemark, J. H. *Topic in Inorganic and Organometallic Stereochemistry*; Geoffroy, G. L., Ed.; Topics in Stereochemistry, Vol. 12; Allinger, N. L., Eliel, E. L., series Eds.;; Wiley: New York, 1981, 155. (c) Westcott, B. L.; Enemark, J. H. In *Inorganic Electronic Structure and Spectroscopy*; Solomon, E. I., Lever, A. B. P., Eds.; Wiley: New York, 1999; Vol. II, p 403.
(9) Wells, F. V.; McCann, S. W.; Wickman, H. H.; Kessel, S. L.; Hendrickson, D. N.; Feltham, R. D. *Inorg. Chem.* **1982**, *21*, 2306.
(10) Feig, A.; Bantista, M. T.; Lippard, S. J. *Inorg. Chem.* **1996**, *35*, 6892.
(11) Pohl, K.; Wieghardt, K.; Nuber, B.; Weiss, J. *J. Chem. Soc., Dalton Trans.* **1987**, 187.
(12) Brown, C. A.; Pavlosky, M. A.; Westre, T. E.; Zhang, Y.; Hedman, B.; Hodgson, K. O.; Solomon, E. I. *J. Am. Chem. Soc.* **1995**, *117*, 715. (b) Westre, T. E.; Di Cicco, A.; Filipponi, A.; Natoli, C. R.; Hedman, B.; Solomon, E. I.; Hodgson, K. O. *J. Am. Chem. Soc.* **1994**, *116*, 6757.

10.1021/ja994161i CCC: $19.00
Published on Web 04/22/2000

Table 1. Selected Spectral Parameters for $\{Fe-NO\}^7$ ($S = {}^3/_2$) Systems

	CN[e]	δ, mm s^{-1} [a]	ΔE_Q, mm s^{-1} [b]	α(Fe−NO), deg[c]	ν(NO), cm^{-1} [d]	ref
proteins						
protocatechuate 4,5-dioxygenase/substrate	6	0.66	−1.67			1
deoxyhemerythrin	6	0.68	+0.61			2,3
deoxyhemerythrin F−NO		0.77	1.03[f]			3
putidamonooxin/substrate		0.68	−1.4			4
ribonucleotide reductase	6	0.70	−1.7			5
isopenicillin N synthase	6	0.75	−1.0			6,7
isopenicillin N synthase-ACV	6	0.65	−1.2			7
model complexes						
[Fe(5-Cl-salen)(NO)]	5	0.654	0.575[f]	147(298 K), 127(175 K)		9
$[LFe(NO)(N_3)_2]$	6	0.62	−1.28	155.6	1690,1712	this work
[Fe(EDTA)(NO)]	5	0.66	−1.67	156(5)	1776	1
$[Fe_2(NO)_2(Et\text{-}HPTB)(O_2CPh)](BF_4)_2$	6	0.67	1.44[f]	167	1785	10
cis-[(cyclam)Fe(NO)I]I (**2**)	6	0.64	−1.78		1726	this work

[a] Isomer shift at 80 K (or below). [b] Quadrupole splitting. [c] Bond angle from X-ray or EXAFS. [d] NO stretching frequency. [e] CN = coordination number. [f] Sign not determined

Table 2. Selected Complexes of the $\{Fe-NO\}^7$ ($S = {}^1/_2$) Type and EPR Spectra

				$A(^{14}N_{NO})$, G			
complex	g_1	g_2	g_3	A_1	A_2	A_3	ref
HbNO	2.082	2.0254	1.9909		27.1	19.3	14e
MbNO	2.0728	2.0068	1.9850		18.6		14d
[(tpp)Fe(NO)]	2.102	2.064	2.010	12.6	17.2	17.3	13a
[(tpp)Fe(NO)(pip)]	2.080.	2.040	2.003			21.7	13a
$[(tim)Fe(NO)(CH_3CN)]$	2.02	1.99	1.97			24.0	13b
$[(i\text{-}mnt)Fe(NO)]^{2-}$	2.043	2.039	2.031	16.0	14.5	12.2	13c
$[(Me_2dtc)_2Fe(NO)]$	2.046	2.039	2.028	12.6	12.2	14.9	13c,d
$[(E_2dtc)_2Fe(NO)]$	2.039	2.035	2.025	13.4	12.1	15.5	13e,f
$[(das)_2Fe(NO)Br]^+$	2.015		1.988				13g
$[(TpivPP)Fe(NO)(NO)_2]^-$	2.085	2.032	2.01	24	16.5	16	51
spin crossover systems	$S = {}^3/_2 \rightleftharpoons S = {}^1/_2$						
$[(tmc)Fe(NO)]^{2+}$							21
[(Salen)Fe(NO)]							9, 13h
[(Salophen)Fe(NO)]							13i

spectroscopy) and calculations which favor a bonding model which invokes high-spin Fe^{III} ($S = {}^5/_2$) antiferromagnetically coupled to NO^- ($S = 1$) yielding the observed $S = {}^3/_2$ ground state, Rodriguez et al.[3] have pointed out that the observed isomer shift in the Mössbauer spectra of $\{Fe-NO\}^7$ complexes is intermediate between that of octahedral ferric and ferrous species. Their density functional theoretical calculations has allowed them to trace these unusual isomer shifts to "strong valence electron delocalization within the $\{Fe-NO\}^7$ unit, whereby some electrons are almost equally shared by metal (i.e. d_{xz} and d_{yz}) and NO π^* orbitals."

It has been stated repeatedly in the literature that Mössbauer parameters and, specifically, the isomer shift do not readily allow the assignment of formal oxidation states in nitrosyliron complexes.[8,10] In no instance has a complete series of isostructural octahedral complexes containing the three $\{Fe-NO\}^{6,7,8}$ moieties been systematically investigated by this spectroscopic method.

Similarly, $\{Fe-NO\}^7$ complexes with an $S = {}^1/_2$ ground state have been reported in the literature (Table 2).[13] The nitrosyl derivatives of myo- and hemoglobin (MbNO, HbNO) have also been reported to possess an $S = {}^1/_2$ ground state.[14] Five- and six-coordinate species of this type have been structurally characterized but little advanced Mössbauer spectroscopic data are available to date. A few cases of $\{Fe-NO\}^7$ species which exhibit high-spin ($S = {}^3/_2$) $\rightleftharpoons$ low-spin ($S = {}^1/_2$) equilibria have also been reported and structurally characterized.

Our strategy to gain a better understanding of the electronic structure of such species has been to design and synthesize a series of "isostructural" complexes and study each member by a combination of spectroscopic methods including a detailed variable-temperature Mössbauer investigation in zero and applied fields.

In a recent paper[15] we have shown that the isomer shift of a series of iron complexes of the Werner type decreases linearly with increasing formal oxidation state: *trans*-$[(cyclam)Fe^{II}(N_3)_2]^0$ ($S = 0$), *trans*-$[(cyclam)Fe^{III}(N_3)_2]^+$ ($S = {}^1/_2$), $[(cyclam)(N_3)Fe^{III}{=}N{=}Fe^{IV}(cyclam)(N_3)]^{2+}$ ($S = {}^1/_2$ and ${}^3/_2$ isomers), and $[(cyclam)Fe^{V}(N)(N_3)]^+$ ($S = {}^3/_2$) where cyclam is the macrocyclic amine 1,4,8,11-tetraazacyclotetradecane. Note that in this series the d^n electron configuration of the iron ion varies systematically by one-electron steps from t^6_{2g} to t^3_{2g} (in O_h symmetry) and all complexes contain an octahedral FeN_6 coordination polyhedron. In the latter two species the strong

(13) Wayland, B. B.; Olson, L. W. *J. Am. Chem. Soc.* **1974**, *96*, 6037. (b) Chen, Y.; Sweetland, A.; Shepherd, R. E. *Inorg. Chim. Acta* **1997**, *260*, 163. (c) Möller, E.; Sieler, J.; Kirmse, R. *Z. Naturforsch.* **1997**, *52b*, 919. (d) Feltham, R. D.; Crain, H. *Inorg. Chim. Acta* **1980**, *40*, 37. (e) Doodman, B. A.; Raynor, J. B.; Symons, M. C. R. *J. Chem. Soc.* **1969**, 2572. (f) Guzy, C. M.; Raynor, J. B.; Symons, M. C. R. *J. Chem. Soc. A* **1969**, 2987. (g) Enemark, J. H.; Feltham, R. D.; Huie, B. T.; Johnson, P. L.; Bizot Swedo, K. *J. Am. Chem. Soc.* **1977**, *99*, 3285. (h) Haller, K. J.; Johnson, P. L.; Feltham, R. D.; Enemark, J. H.; Ferraro, J. R.; Basile, L. J. *Inorg. Chim. Acta* **1979**, *33*, 119. (i) Leeuwenkamp, O. R.; Plug, C. M.; Bult, A. *Polyhedron* **1987**, *6*, 295.

(14) Lang, G.; Marshall, W. *Proc. Phys. Soc.* **1966**, *87*, 3. (b) Oosterhuis, W. T.; Lang, G. *J. Chem. Phys.* **1969**, *50*, 4381. (c) Spartalian, K.; Lang, G.; Yonetani, T. *Biochim. Biophys. Acta* **1976**, *428*, 281. (d) Dickinson, L. C.; Chien, C. W. *J. Am. Chem. Soc.* **1971**, *93*, 5036. (e) Chien, J. C. *J. Chem. Phys.* **1969**, *51*, 4220. (f) Saucier, K. M.; Freeman, G.; Mills, J. S. *Science* **1962**, *137*, 752.

(15) Meyer, K.; Bill, E.; Mienert, B.; Weyhermüller, T.; Wieghardt, K. *J. Am. Chem. Soc.* **1999**, *121*, 4859.

nitrido π-donor ligand is present whereas in the former two this is not the case. Clearly, the Mössbauer isomer shift is an excellent marker for the given d^n electron configuration at the iron ion.

In this work we report a related series of octahedral nitrosyliron complexes, namely *trans*-[(cyclam)Fe(NO)Cl]-(ClO_4) [an $\{Fe-NO\}^7$ ($S = {}^1/_2$) species], *cis*-[(cyclam)Fe(NO)I]I [an $\{Fe-NO\}^7$ ($S = {}^3/_2$) species], *trans*-[(cyclam)Fe(NO)Cl]$^{2+}$ [an $\{Fe-NO\}^6$ ($S = 0$) species], and *trans*-[(cyclam)Fe(NO)I]^0 [an $\{Fe-NO\}^8$ ($S = 0$) species]. We have spectroscopically (UV−vis, EPR, Mössbauer) characterized their electronic structures. The results show that Mössbauer spectroscopy is a valuable tool for the correct assignment of oxidation levels.

Experimental Section

The ligand 1,4,8,11-tetraazacyclotetradecane (cyclam)[16] and complexes *cis*-[(cyclam)Fe(Cl_2)]Cl[17] as well as [LFe(NO)(N_3)$_2$][11] have been prepared as decribed in the literature.

***cis*-[(cyclam)$^{56/57}$Fe(Cl_2)]Cl.** To prepare ^{57}Fe isotopically enriched complexes the starting material *cis*-[(cyclam)$^{56/57}$Fe(Cl_2)]Cl was synthesized as follows. ^{57}Fe (34.4 mg) and ^{56}Fe (59.9 mg) foil was dissolved in concentrated hydrochloric acid in the presence of air by heating to reflux. The clear solution was dried in vacuo and the $^{56/57}FeCl_3$ residue was dissolved in dry methanol (10 mL). Addition of the ligand cyclam (0.46 g; 2.44 mmol) and heating to reflux for 1 h produced a dark yellow solution that was cooled to 20 °C. Dropwise addition of 30% HCl initiated the precipitation of brown microcrystalline *cis*-[(cyclam)$^{56/57}$Fe(Cl_2)]Cl (35% ^{57}Fe), which was filtered off. Further addition of HCl to the solution produced colorless crystals of [H_2cyclam]Cl_2 which were removed by filtration. Further addition of HCl yielded another crop of crystalline *cis*-[(cyclam)$^{56/57}$Fe(Cl_2)]Cl. Yield: 0.55 g (90%).

***trans*-[(cyclam)Fe(NO)(Cl)](ClO_4) (1).** To a solution of *cis*-[(cyclam)-Fe(Cl_2)]Cl (0.20 g; 0.55 mmol) in water (20 mL) was added solid [NH_3OH]Cl (1.15 g; 16.5 mmol) whereupon the starting complex *cis*-[(cyclam)FeCl_2]Cl started to precipitate again. To this yellow suspension was added dropwise 1.0 M aqueous NaOH with stirring at ambient temperature until at pH 6−7 a deep blue clear solution was obtained. The color of this solution changed within 5 min to brown-red. Addition of $NaClO_4$ (2.0 g) initiated the precipitation of brown microcrystals of **1**. Yield: 0.08 g (36%). Slow recrystallization of the crude material from acetonitrile solution produced single crystals of **1** suitable for X-ray crystallography. Anal. Calcd for $C_{10}H_{24}N_5O_5FeCl_2$: C, 28.50; H, 5.74; N, 16.63. Found: C, 28.3; H, 5.7; N, 16.3.

***cis*-[(cyclam)Fe(NO)(I)]I (2).** To a suspension of *cis*-[(cyclam)Fe-(Cl_2)]Cl (0.20 g; 0.55 mmol) and [NH_3OH]Cl (1.15 g) in water (10 mL) was added NaI (3.0 g; 20 mmol). Immediately after the addition of NaI an aqueous solution of 1.0 M NaOH was added dropwise with stirring (pH 6−7) until from the reddish reaction mixture dark green microcrystals precipitated which were rapidly filtered off, washed with cold ethanol and diethyl ether, and air-dried. Yield: 0.20 g (67%). Anal. Calcd for $C_{10}H_{24}N_5OI_2Fe$: C, 22.24; H, 4.48; N, 12.97. Found: C, 22.1; H, 4.3; N, 12.8.

[L′Fe(NO)(ONO)(NO_2)](ClO_4). A solution of L′$FeCl_3$ (0.8 g), where L′ represents 1,4,7-triazacyclononane, and $NaNO_2$ (7.5 g) in 0.10 M aqueous hydrochloric acid (120 mL) was stirred at ambient temperature for 1.5 h. To the filtered brown solution was added $NaClO_4 \cdot H_2O$ (2.5 g). Upon storage at 0 °C for 12 h a brown crystalline precipitate formed which was collected by filtration. Yield: 0.46 g. Anal. Calcd for C_6H_{15}-$ClFeN_6O_9$: C, 17.73; H, 3.72; N, 20.67. Found: C, 17.5; H, 3.7; N, 20.7.

X-ray Crystallographic Data Collection and Refinement. A brown-violet single crystal of **1** and a brown crystal of [L′Fe(NO)-(ONO)(NO_2)](ClO_4) were sealed in a glass capillary and mounted on a Siemens SMART CCD-detector diffractometer equipped with a cryogenic nitrogen cold stream at 100 K, respectively. Graphite monochromated Mo Kα radiation ($\lambda = 0.71073$ Å) was used. Intensity data were collected by hemisphere runs taking frames at 0.30° in ω. The data sets were corrected for Lorentz and polarization effects and for **1** a semi-empirical absorption correction was carried out using the program SADABS.[18] Crystallographic data are listed in Table 3. The Siemens ShelXTL[19] software package was used for solution, refinement and artwork of the structures. All non-hydrogen atoms were refined with anisotropic displacement parameters. The hydrogen atoms were placed at calculated positions and refined as riding atoms.

Table 3. Crystallographic Data for *trans*-[(cyclam)Fe(NO)Cl]ClO_4 (**1**) and [L′Fe(NO)(NO_2)$_2$](ClO_4)

	1	[L′Fe(NO)(NO_2)$_2$](ClO_4)
chem formula	$C_{10}H_{24}Cl_2FeN_5O_5$	$C_6H_{15}ClFeN_6O_9$
FW	421.09	406.54
space group	*Pbca*	*Pn*
a, Å	13.010(2)	13.450(2)
b, Å	10.853(1)	8.1261(8)
c, Å	23.692(4)	13.478(2)
β, deg	90^o	109.43(2)
V, Å^3	3345.3(8)	1389.2(3)
Z	8	4
T, K	100(2)	100(2)
ρ_{calc}, g cm^{-3}	1.672	1.944
diffractometer used	Siemens SMART	Siemens SMART
λ(Mo Kα), Å	0.71073	0.71073
μ, cm^{-1}	12.52	13.41
no. of data	21031	8915
no. of unique data	3528	5814
no. of parameters/ restraints	244/0	439/47
*R*1[a]; *wR*2 (all data)[b]	0.054; 0.124	0.046; 0.1207

[a] $R1 = \sum(|F_o| - |F_c|)/\sum|F_o|$ observation criterion: $I > 2\sigma(I)$. [b] $wR2 = [\sum[w(F_o^2 - F_c^2)^2]/\sum[w(F_o^2)^2]^{1/2}$ where $w = 1/\sigma^2(F_o^2) + (aP)^2 + bP$, $P = (F_o^2 + 2F_c^2)/3$.

The oxygen atoms of the perchlorate anion in **1** were found to be disordered over two sites. The two sets of atoms were refined with occupancy factors of 0.67 and 0.33, respectively. A weak hydrogen bridge between the cation and the perchlorate anions in **1** gives rise to a slight disorder of the iron complex. This results in abnormally large thermal parameters for all atoms not lying on the Cl−Fe−N_{NO} axis of the complex.

One of the two crystallographically independent cations in [L′Fe-(NO)(ONO)(NO_2)](ClO_4) displays a disorder of the carbon atoms of the 1,4,7-triazacyclononane backbone. This disorder was successfully modeled by a split atom model for these C atoms with occupancy factors of 0.65 and 0.35, respectively.

Physical Measurements. The equipment used for IR, UV−vis, Mössbauer, and EPR spectroscopy has been described in ref 15. Low-temperature EPR, magnetic Mössbauer spectra, and magnetization measurements were analyzed on the basis of a spin-Hamiltonian description of the electronic ground-state spin multiplet as is described in detail also in ref 15.

Results

Preparation and Characterization of Complexes. To obtain a deeper understanding of the electronic structures of a series of octahedral complexes containing the $\{Fe-NO\}^{6,7,8}$ structural motif as electronically unperturbed by the co-ligands as possible, we used the redox-innocent macrocycles 1,4,7-trimethyl-1,4,7-triazacyclononane (L) in the previously synthesized and structurally characterized complex [LFe(NO)(N_3)$_2$] [11] ($\{Fe-NO\}^7$, $S = {}^3/_2$) and triazacyclononane (L′) in [L′Fe(NO)(ONO)-(NO_2)]$ClO_4$11 ($\{Fe-NO\}^6$, $S = 0$), and in this work, 1,4,8,11-tetraazacyclotetradecane (cyclam).

From the reaction of *cis*-[(cyclam)Fe(Cl_2)$_2$]Cl, a high-spin ferric precursor,[17] with hydroxylamine in water at 20 °C we

(16) Barefield, K. E.; Wagner, F. *Inorg. Synth.* **1976**, *16*, 220.
(17) Chan, P.-K.; Poon, C.-K. *J. Chem. Soc., Dalton Trans.* **1976**, 858.
(18) SADABS, Sheldrick, G. M., Universität Göttingen, 1994.
(19) ShelXTL V. 5.0; Siemens Analytical X-ray Instruments, Inc. Maddison, WI.

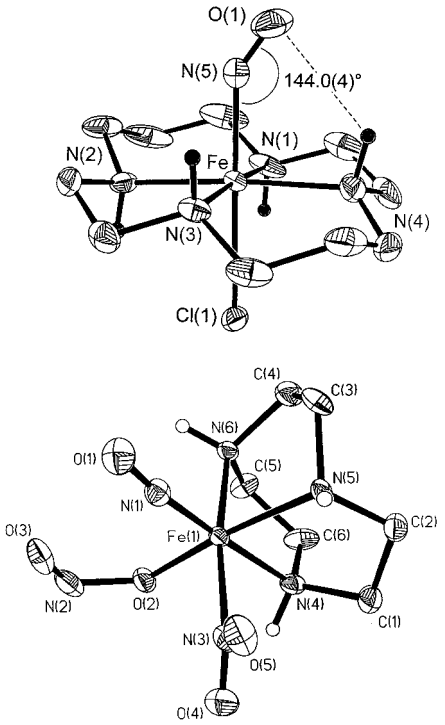

Figure 1. Perspective view of the monocation in crystals of **1** (top) and of one crystallographically independent cation in crystals of [L′Fe(NO)(ONO)(NO_2)](ClO_4) (bottom). Small circles represent N−H protons while those of the methylene groups are not shown.

obtained upon addition of $NaClO_4$ brown microcrystals of *trans*-[(cyclam)Fe(NO)(Cl)](ClO_4) (**1**). Using similar reaction conditions but adding NaI instead of $NaClO_4$ and performing the precipitation and workup more rapidly we obtained green microcrystals of *cis*-[(cyclam)Fe(NO)I]I (**2**).

The cis and trans configuration of the coordinated ligand cyclam in **2** and **1**, respectively, was clearly established by their infrared spectra.[20] For **1** a single *out-of-plane* wagging mode, γ(N−H) at 888 cm^{-1}, and a *single* rocking mode, $\delta(CH_2)$ at 808 cm^{-1}, have been observed indicative of the trans configuration. In contrast, for **2** *two* frequencies are observed for each of these modes: γ(N−H) 862, 852, and $\delta(CH_2)$ 805, 793 cm^{-1}. The ν(NO) stretching frequency has been detected at 1611 cm^{-1} for **1** and 1726 cm^{-1} for **2**.

Complex **2** must be rapidly precipitated from solution. We have found that these preparations invariably are contaminated with ∼10% *cis*-[(cyclam)$Fe^{III}(I)_2$]I ($S = {}^5/_2$). It is not possible to purify **2** by fractional recrystallization because **2** isomerizes fairly rapidly even at lower temperatures within a few seconds yielding a trans-configurated species.

The crystal structure of **1** has been determined by single-crystal X-ray crystallography at 100(2) K. Figure 1 shows the structure of the monocation in crystals of **1** and Table 4 gives selected bond distances and angles. The cyclam ligand is bound in its strain-free trans-III or *two-up/two-down* configuration to the central iron ion (R, S, S, R configuration at the chiral nitrogen atoms). The average Fe−N_{amine} bond distance at 2.03 ± 0.01 Å is in excellent agreement with simple low-spin ferric complexes of the type *trans*-[(cyclam)$Fe^{III}(X)_2$]$^+$. For example, for X = N_3^- an average Fe−N_{amine} distance of 2.00 ± 0.01 Å has recently been determined.[15] The coordinated nitrosyl forms a bent Fe−NO moiety with a bond angle at 144.0(4)°. The Fe−N_{NO} bond at 1.820(4) Å indicates considerable double bond character. The iron ion is bound in the *in-plane* mode; the Fe ion is displaced by only 0.086 Å from the best plane defined by the four amine nitrogens which deviate by an average of only 0.004 Å from this plane. The sixth coordination site in **1** is occupied by a loosely bound chloride ion with an Fe−Cl bond length of 2.456(1) Å.

(20) Poon, C.-K. *Inorg. Chim. Acta* **1970**, *5*, 322.

Table 4. Selected Bond Distances (Å) and Angles (deg) of **1** and [L′Fe(NO)(ONO)(NO_2)](ClO_4)

Complex **1**			
Fe−N1	2.005(3)	Fe−N5	1.820(4)
Fe−N2	2.007(3)	Fe−Cl	2.456(1)
Fe−N3	2.010(3)	N5−O1	1.006(4)
Fe−N4	1.996(3)	Fe−N5−O1	144.0(4)
Complex [L′(NO)(ONO)(NO_2)](ClO_4)			
Fe1−N1	1.644(4)	Fe1−N6	1.999(4)
Fe1−O2	1.914(3)	N1−O1	1.163(5)
Fe1−N3	1.969(4)	N2−O3	1.216(6)
Fe1−N4	1.993(4)	N2−O2	1.322(5)
Fe1−N5	1.996(4)	N3−O4	1.216(6)
Fe1−O2−N2	125.1(3)	N3−O5	1.282(5)
O2−N2−O3	116.3(4)	Fe1−N1−O1	171.2(4)
O4−N3−O5	122.4(4)	Fe1−N3−O4	120.9(4)
		Fe1−N3−O5	116.6(4)

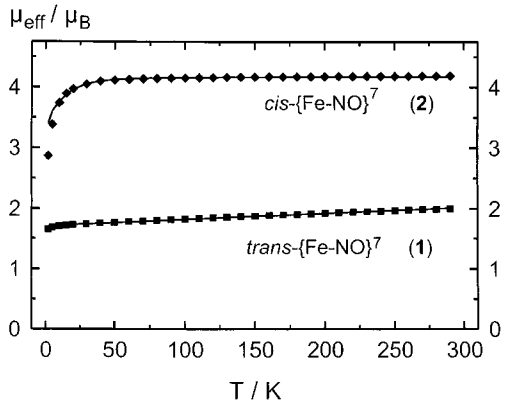

Figure 2. Temperature dependence of magnetic moments, μ_{eff}/μ_B, of solid samples of **1** and **2**. The solid lines represent best fits using the parameters given in the text.

The electronic ground states of **1** and **2** have been established from variable-temperature and variable-field susceptibility measurements by using a SQUID magnetometer. Figure 2 shows the temperature dependence of the effective magnetic moments of **1** and **2** in an external magnetic field of 1 T and a best fit of the data. Both species are paramagnetic. The fit shown in Figure 2 for **1** has been obtained by using the following parameters: a fixed $g = 2.012$ which was determined from EPR measurements (see below) and a temperature-independent paramagnetism, χ_{TIP}, of 483 × 10^{-6} cm^3 mol^{-1}. Thus **1** possesses an $S = {}^1/_2$ ground state of {Fe−NO}^{7}. In contrast, complex **2** exhibits an $S = {}^3/_2$ ground state. The fit of the data in Figure 2 was obtained by including 12% of a paramagnetic impurity of *cis*-[(cyclam)$Fe^{III}(I)_2$]I ($S = {}^5/_2$) as was determined from Mössbauer spectroscopy (see below). The marked decrease of the magnetic moment of **2** at temperatures <50 K is due to a large zero-field splitting of **2** which was modeled with $D_{3/2} = +12.6$ cm^{-1} in agreement with Mössbauer spectroscopic simulations for an $S = {}^3/_2$ ground state. In conjunction with the simulations of the magnetic Mössbauer spectra we remeasured also the magnetic susceptibility of the $S = {}^3/_2$ complex [LFe(NO)(N_3)$_2$][11] by using variable fields (1, 4, 7 T). In contrast to the very large value $D_{3/2} = 20$ cm^{-1} reported previously,[12a] our data are best described with a ZFS of $D_{3/2} = +13.6$ cm^{-1} (Figure S1, Supporting Information).

Structurally characterized octahedral $\{Fe-NO\}^6$ complexes are extremely rare. [(tmc)Fe(NO)(OH)](ClO_4) (tmc = tetramethylcyclam) represents an early example which has not been spectroscopically characterized due to its somewhat problematic synthetic accessibility.[21] In 1986 we had described the synthesis of [L′Fe(NO)(NO_2)$_2$](ClO_4)·2H_2O but at that time did not obtain single crystals.[11] From its infrared spectrum we concluded that this species contains a nitrosyl(dinitro)iron core: ν(N═O) 1890; $\nu_{as}(NO_2)$ 1430; and $\nu_s(NO_2)$ 1310 cm^{-1}. In an attempt to grow single crystals we have now obtained an isomer of this complex containing the nitrosyl(nitrito)nitroiron core, namely, [L′Fe(NO)(ONO)(NO_2)](ClO_4). In the infrared two ν(NO) stretching frequencies at 1907 and 1885 cm^{-1} are observed; the O-coordinated nitrito ligand gives rise to two ν(N═O) stretching frequencies at 1477 and 1464 cm^{-1}, and the N-coordinated nitro group displays N−O stretching frequencies $\nu_{as}(NO_2)$ at 1439, 1419 and $\nu_s(NO_2)$ at 1315, 1306 cm^{-1}. [L′Fe(NO)(ONO)(NO_2)](ClO_4) is diamagnetic indicating an $S = 0$ ground state.

The crystal structure determination reveals that two crystallographically independent cations [L′Fe(NO)(ONO)(NO_2)]$^+$ are present in the crystals. The cation possesses two sources of chirality. The iron ion is a center of chirality giving rise to Δ, Λ configurations, and the three five-membered Fe−N−C−C−N chelate rings of the 1,4,7-triazacyclononane ligand adopt either a ($\lambda\lambda\lambda$) or a ($\delta\delta\delta$) conformation. Thus the diastereomers Δ($\lambda\lambda\lambda$) and Δ($\delta\delta\delta$) and their respective enantiomers (Λ($\delta\delta\delta$), Λ($\lambda\lambda\lambda$) are present in equal amounts in the crystals. The latter are interrelated by a crystallographic gliding mirror plane. Figure 1 (bottom) shows the structure of one of these cations [L′Fe(NO)(ONO)(NO_2)]$^+$ containing a nearly linear $\{Fe-NO\}^6$ moiety, an O- and an N-coordinated nitrito and a nitro group, respectively. Table 4 gives selected bond distances and angles. The most salient feature of this structure are the short $Fe-N_{amine}$ distances at an average 1.996 Å which are slightly shorter than those in **1**, an $\{Fe-NO\}^7$ ($S = {}^1/_2$) species with av. $Fe-N_{amine}$ = 2.004 Å) and much shorter than those in [LFe(NO)(N_3)$_2$], an $\{Fe-NO\}^7$ ($S = {}^3/_2$) species with av. 2.252 Å. For comparison, in the low-spin ferrous and ferric species $[L'_2Fe]^{2+/3+}$ the average $Fe-N_{amine}$ distance is found at 2.03 and 1.99 Å,[22] respectively, whereas this distance is >2.10 Å in all octahedral high-spin ferric and >2.20 Å in high-spin ferrous species. These observations lend strong support to the notion that [LFe(NO)(N_3)$_2$] ($S = {}^3/_2$) contains a high-spin ferric ion whereas in **1** the e_g metal orbitals (in O_h symmetry) must, at least partly, be unoccupied as in a low or intermediate spin ferric ion. On extrapolation of this argument we conclude that a low-spin Fe^{IV} ion ($S = 1$) may be present in [L′Fe(NO)(ONO)(NO_2)]$^+$. The diamagnetic ground state is then attained by intramolecular antiferromagnetic coupling of this Fe^{IV} ion to an NO^- ($S = 1$) ligand.

Electro- and Spectroelectrochemistry. Figure 3 displays the cyclic and square-wave voltammograms of **1** in acetonitrile (0.10 M [(n-Bu)$_4$N]PF_6) at 20 °C. In the following all redox potentials are given vs the ferrocenium/ferrocene couple (Fc^+/Fc). Clearly, two reversible one-electron-transfer waves are detected where the process at $E_{1/2} = 0.14$ V corresponds to a one-electron oxidation generating *trans*-[(cyclam)Fe(NO)Cl]$^{2+}$ and that at −1.30 V is due to a reversible one-electron reduction affording *trans*-[(cyclam)Fe(NO)Cl]^0 as was established from coulometric measurements at appropriately fixed potentials. Thus **1** exists

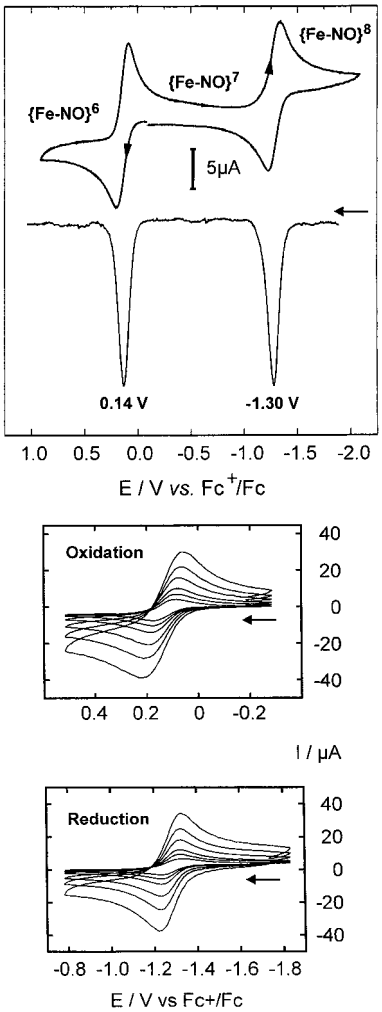

Figure 3. Cyclic (top) and square-wave (middle) voltammograms of **1** in acetonitrile at 298 K (0.10 M [(n-Bu)$_4$N]PF_6 supporting electrolyte, glassy carbon working electrode, reference electrode Ag/$AgNO_3$). The potentials are referenced vs the ferrocenium/ferrocene (Fc^+/Fc) couple. Bottom: Cyclic voltammograms of the oxidation and reduction wave, respectively, at scan rates 2.0, 1.0, 0.50, 0.20, 0.10, and 0.05 V s^{-1}, respectively.

in three different oxidation levels, namely a dicationic $\{Fe-NO\}^6$, a monocationic $\{Fe-NO\}^7$, and a neutral $\{Fe-NO\}^8$ species. From the coulometric measurements it was established that the oxidized $\{Fe-NO\}^6$ species is stable at ambient temperature for at least 2 h whereas the reduced $\{Fe-NO\}^8$ form is only stable at −30 °C. Hence the oxidized and reduced species were readily investigated in solution by UV−vis, EPR, and Mössbauer spectroscopy.

Figures 4 and 5 show the results of the spectroelectrochemical oxidation of **1** at 20 °C and of the corresponding reduction at −30 °C. The electronic spectrum of **1** in CH_3CN displays two absorption maxima in the visible at 398 (ϵ = 300 M^{-1} cm^{-1}) and 560 nm (ϵ = 145 M^{-1} cm^{-1}). Upon one-electron oxidation these maxima disappear and a new band at 362 nm (ϵ = 500 M^{-1} cm^{-1}) is generated.

Conversely, upon one-electron reduction of **1** the position of the two absorption maxima of **1** remains unchanged at 398 and 560 nm only their intensity increases to ∼500 and ∼190 M^{-1} cm^{-1}, respectively. This is a remarkable result: the spectra of **1** and *trans*-[(cyclam)Fe(NO)Cl]$^{2+}$ are completely different in nature whereas the spectra of **1** and *trans*-[(cyclam)Fe(NO)Cl]^0 are nearly the same. If one assumes that due to the overall low intensity of all maxima in the visible these transitions are

(21) Hodges, K. D.; Wollmann, R. G.; Kessel, S. L.; Hendrickson, D. N.; Van Derveer, D. G.; Barefield, E. K. *J. Am. Chem. Soc.* **1979**, *101*, 906.

(22) Boeyens, J. C. A.; Forbes, A. G. S.; Hancock, R. D.; Wieghardt, K. *Inorg. Chem.* **1985**, *24*, 2926−2931.

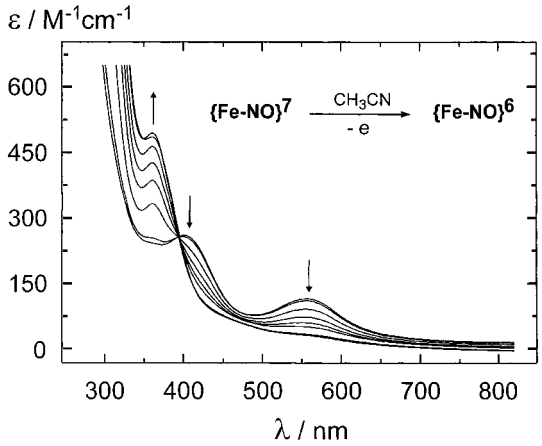

Figure 4. Spectroelectrochemical changes observed during the one-electron oxidation of **1** in CH_3CN at 298 K. The arrows indicate the appearance or disappearance of peaks during the oxidation.

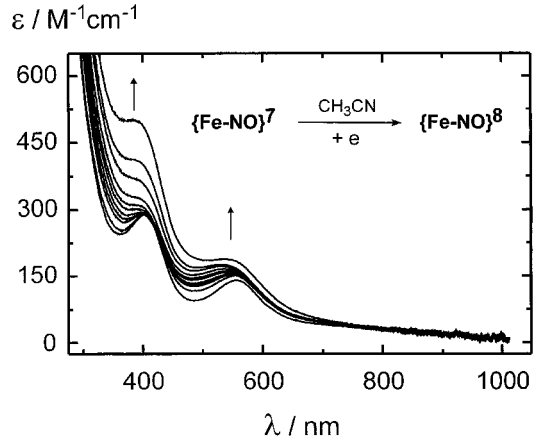

Figure 5. Spectroelectrochemical changes observed during the one-electron reduction of **1** in CH_3CN at −30 °C. The arrows indicate the increase in absorbance during reduction.

predominantly of d−d character, one arrives at the conclusion that the $\{Fe-NO\}^7$ and $\{Fe-NO\}^8$ species have a rather similar d^n configuration implying that the added electron resides in a π^*(NO) ligand orbital. In contrast, $\{Fe-NO\}^6$ and $\{Fe-NO\}^7$ must then have different d^n electron configurations. In other words, the one-electron oxidation of **1** may be considered to be metal-centered and the one-electron reduction to be ligand-centered (NO).

We have also performed a coulometric one-electron oxidation and a one-electron reduction of **1** dissolved in dimethyl sulfoxide (dmso) at ambient temperature in a thin-layer electrochemical cell and recorded the infrared spectra in the range 1500−2000 cm^{-1}. For the parent complex **1** the ν(NO) stretching frequency is observed at 1620 cm^{-1} which upon oxidation disappears and a new band at 1902 cm^{-1} is observed which we assign to the $\{Fe-NO\}^6$ species *trans*-$[(cyclam)Fe(NO)Cl]^{2+}$. Similarly, upon one-electron reduction of **1** at −20 °C the 1620 cm^{-1} mode disappears but we have not been able to identify a new ν(NO) stretching frequency for the generated $\{Fe-NO\}^8$ species in our experimental spectral window. Under our experimental setup using dmso as solvent this implies that this ν(NO) frequency must be below 1500 cm^{-1}. When the fully oxidized or reduced species were rereduced or reoxidized, respectively, the ν(NO) mode of **1** at 1620 cm^{-1} was fully regenerated indicating the reversibility of the process. It is noted that for $[(tmc)Fe(NO)(OH)](ClO_4)_2 \cdot CH_3CN$ which represents the first structurally characterized example for an octahedral $\{Fe-NO\}^6$ species ($S = 0$) the ν(NO) mode has been observed at 1890 cm^{-1} (tmc = tetramethylcyclam).[21] Scheidt et al.[23] report a ν(NO) at 1937 cm^{-1} for six-coordinate $[Fe(TPP)(NO)(H_2O)](ClO_4)$, also an octahedral $\{Fe-NO\}^6$ species.[23] For $[L'Fe(NO)(ONO)(NO_2)](ClO_4)$ two ν(NO) bands at 1907 and 1885 cm^{-1} corresponding to the two crystallographically independent cations have been observed.

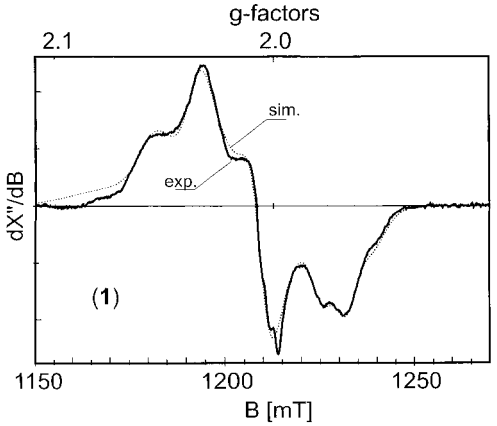

Figure 6. Q-band EPR spectrum of **1** in a CH_3CN/CH_3OH (2:1) mixture at 50 K. Conditions: ν = 33.923 GHz; power 0.1 mW, modulation amplitude 2 mT. Simulation parameters are given in the text. Gaussian lines with angular- and m_I-dependent widths were used with parameters W = (0.2, 0.2, 6.) mT, C_1 = (0.36, 0.37, −1.) mT/GHz, and C_2 = (20.7, 5.4, 6.9) mT.[28]

On the other hand, the well-characterized diamagnetic $\{Fe-NO\}^8$ ($S = 0$) species containing a linear Fe−NO moiety in, for example, $[L_4Fe(NO)]^+$ (L = $P(OMe)_3$, $P(OEt)_3$),[24] $[Fe(NO)(np_3)]$ (np_3 = tris(2-diphenylphosphinoethyl)amine),[25] and other five-coordinate organometallic phosphine complexes[26,27] displays ν(NO) bands in the region ∼1730 ± 20 cm^{-1}. If our reduced *trans*-$[(cyclam)Fe(NO)Cl]^0$ would be of this type we would have detected its ν(NO) band using the above spectroelectrochemical conditions. Thus these experiments point to a different electronic structure of the reduced form of **1**.

EPR Spectroscopy. The X-band EPR spectrum of **1** in a frozen solution of acetonitrile at 10 K displays a broad (13.5 mT) isotropic signal at g_{iso} = 2.012. It appears that intermolecular dipolar spin couplings broaden the spectra and reduce the spectral resolution, even in diluted samples (≈50 μM). However, at higher frequency (Q-band) the higher resonance fields apparently decouple the molecular spins so that a reasonably well resolved EPR spectrum of **1** was obtained. The spectrum is shown in Figure 6. The simulation was achieved by involving first-order hyperfine interaction to one nitrogen (of the NO ligand) (^{14}N, I = 1) with the parameters g_x = 2.0520, g_y = 2.0145, g_z = 1.9698 and $A(^{14}N)$ = (112, 49.9, 59.1) × 10^{-4} cm^{-1} (117, 53, 64 G) with angular- and m_I-dependent Gaussian line shapes.[28] This spectrum is remarkably similar to those reported for many five-coordinate $\{Fe-NO\}^7$ species with an $S = {}^1/_2$ ground state containing porphinato and dithiocarbamato ligands (Table 2). Interestingly, it also resembles closely spectra recorded for HbNO and MbNO.[14d,e] The large anisotropy of the line width is characteristic for $\{Fe-NO\}^7$ species

(23) Scheidt, W. R.; Lee, Y. J.; Hatano, K. *J. Am. Chem. Soc.* **1984**, *106*, 3191.
(24) Albertin, G.; Bordignon E. *Inorg. Chem.* **1984**, *23*, 3822.
(25) Di Vaira, M.; Ghilardi, C. A.; Sacconi, L. *Inorg. Chem.* **1976**, *15*, 1555.
(26) Johnson, B. F. G.; Segal, J. A. *J. Chem. Soc., Dalton Trans.* **1972**, 1268.
(27) Hoffman, P. R.; Miller, J. S.; Ungermann, C. B.; Caulton, K. J. *J. Am. Chem. Soc.* **1973**, *95*, 7902.

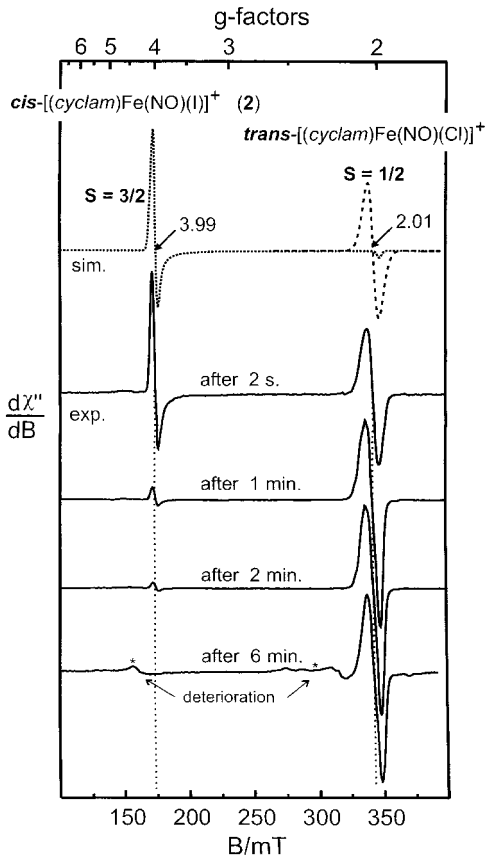

Figure 7. X-band EPR spectra of **2** in CH_3OH at 3.0 K as a function of warm-up and freeze-quench experiments showing the isomerization **2** → **1**. Conditions: $\nu = 9.645$ GHz; power 2.0×10^{-4} mW, modulation amplitude 11.4 G. Simulation parameters are given in the text.

containing four equatorial nitrogen donors. In general, smaller line widths are observed in the direction of the Fe−NO vector as compared to the plane of four ligand nitrogen donors. In **1** additional coupling to protons of the secondary amine ligand cyclam can cause a further increase in line width.

The $S = {}^3/_2$ ground state of the {Fe−NO}^{7} complex **2** has been investigated by X-band EPR spectroscopy both in the solid state and frozen methanol solution in the temperature range 3 to 50 K.

Due to fast isomerization of **2** → *trans*-[(cyclam)Fe(NO)(I)]I the solution EPR spectra of **2** have been obtained only by using a special freeze-quench technique. The carefully degassed solvent methanol in an EPR tube was frozen and a few crystals of **2** were added to the frozen solution under an Ar blanketing atmosphere. Upon a very brief warm-up of this mixture in the EPR spectrometer, until the methanol had liquified, these crystals sank slowly to the bottom of the cavity with dissolution of a very small amount of **2**. Then the solution was immediately frozen again and the spectrum was recorded. The result of such an experiment is shown in Figure 7 where this liquify−freeze process was repeated after 1, 2, and 6 min. The first recorded spectrum displays a strong signal at $g \sim 4$ and a weaker isotropic signal at $g = 2.01$. Quantitation of these signals reveals that the latter accounts for 24% of the total intensity; it is assigned to *trans*-[(cyclam)Fe(NO)I]$^+$ with an $S = {}^1/_2$ ground state. This signal becomes the dominant signal; after three warm-ups only this signal is observed. The resonance at $g \sim 4$ has completely vanished.

The signal at $g \sim 4$ is assigned to the $S = {}^3/_2$ ground state of **2** which is quite similar to that reported for [LFe(NO)(N_3)]. The axial spectrum was simulated with effective g values $g_\perp^{\text{eff}} = 3.99$ and $g_\parallel^{\text{eff}} = 1.98$, which are characteristic of the $|m_s = \pm{}^1/_2\rangle$ Kramers doublets in a $S = {}^3/_2$ manifold with large zero-field splitting ($2D_{3/2} \gg \mu B$) and axial symmetry $E/D_{3/2} \approx 0$. A plot of the EPR intensity of **2**, $I \times T$ versus T, is consistent with the magnetic susceptibility result $D_{3/2} = +12.6$ cm^{-1}. Since for axial zero-field symmetry the $|m_s = \pm{}^3/_2\rangle$ Kramers doublet is EPR-silent at X-band, the intensity data are not very sensitive for the numerical value of $D_{3/2}$ but they clearly show that the resonance doublet is a magnetic ground state and, hence, that $D_{3/2}$ is positive. For [LFe(NO)(N_3)$_2$] the zero-field splitting is very similar, $D_{3/2} = +13.6$ cm^{-1}.

Mössbauer Spectroscopy. (a) Isomer Shifts and Quadrupole Splittings. Zero-field Mössbauer spectra on solid samples or frozen solutions of complexes were measured in the temperature range 2−295 K. All complexes show practically symmetric quadrupole doublets in the whole temperature range. The absence of magnetic hyperfine splittings also in the paramagnetic {Fe−NO}^{7} compounds (in the solid state) shows fast electronic spin relaxation with respect to the nuclear precession rates. In this regime the internal fields at the nucleii average to zero without externally applied fields. The obtained zero-field quadrupole spectra were simulated with Lorentzian doublets; the results are summarized in Table 5.

The spectra of [LFe(NO)(N_3)$_2$] and **2** show very similar isomer shifts of 0.62 and 0.64 mm s^{-1} at 4.2 K (Figure S2, Supporting Information). Isomer shifts in the range 0.63−0.78 mm s^{-1} have been observed for all octahedral {Fe−NO}^{7} $S = {}^3/_2$ complexes including the respective sites in metalloproteins such as the nitrosyl derivative of deoxyhemerythrin[2,3] ($\delta = 0.68$ mm s^{-1}) (see Table 1).

Also in line with previous data on octahedral {Fe−NO}^{7} ($S = {}^3/_2$) species is the observed temperature-independence of the quadrupole splitting, ΔE_Q, of [LFe(NO)(N_3)$_2$] and **2** (4.2−295 K). In contrast, the isomer shift, δ, of the two complexes increases slightly by 0.11 mm s^{-1} with decreasing temperature in the range 295−4.2 K, which is probably due to the second-order Doppler effect. For the {Fe−NO}^{7} unit in nitrosyl deoxyhemerythrine the same trend of the same magnitude is observed.[3] This is strong evidence for the notion that the electronic structure is dominated by the common {Fe−NO}^{7} moiety.

The zero-field Mössbauer spectrum of **1** at 80 K also consists of a symmetrical doublet with an isomer shift of 0.27 mm s^{-1} and a quadrupole splitting, $|\Delta E_Q|$, of 1.26 mm s^{-1} (Figure 8, middle). In the temperature range 4.2−80 K both isomer shift and quadrupole splitting are temperature-independent within experimental error.

It is now an important observation that the isomer shift of the cis and trans-"isomers", **2** and **1**, containing an {Fe−NO}^{7} ($S = {}^3/_2$) and an {Fe−NO}^{7} ($S = {}^1/_2$) moiety, respectively, differ by 0.37 mm s^{-1}. For the corresponding high-spin and low-spin forms of five-coordinate [(salen)Fe(NO)] ($S = {}^3/_2 \rightleftharpoons S = {}^1/_2$) this difference is smaller at ~0.16 mm s^{-1}.[9] It is of significance that this difference in isomer shifts at 80 K is 0.56 mm s^{-1} for the high- and low-spin ferrous isomers *cis*-[(cyclam)Fe^{II}(N_3)$_2$] ($S = 2$) and *trans*-[(cyclam)Fe^{II}(N_3)$_2$] ($S = 0$) and 0.17 mm s^{-1} for their high- and low-spin ferric analogues *cis*-[(cyclam)Fe^{III}-

(28) The line widths for the field-swept spectrum are determined according to $\sigma(\text{field}) = \text{sqrt}(\sum_{i=x,y,z}\sigma_i^2 l_i^2)$, where l_i denotes the direction cosines and σ_i the angular dependent line width $\sigma_i^2 = W_i + C_{1,i}\cdot\nu + \sum_{mI}C_{2,i}\cdot m_I^2$, where W_i is the intrinsic residual line width, ν is the microwave frequency, and $m_I = -1, 0, 1$ is the magnetic quantum number of the ^{14}N nucleus ($I = 1$). For further details see for instance: Pilbrow, J. R. *Transition Ion Electron Paramagnetic Resonance*; Clarendon Press: Oxford, 1990.

Table 5. Spin Hamiltonian and Hyperfine Parameters of Complexes at 4.2 K

	[LFe(NO)(N_3)$_2$]	*trans*-[(cyclam)-Fe(NO)Cl]$^+$ (**1**)	*trans*-[(cyclam)-Fe(NO)Cl]$^{2+}$	*trans*-[(cyclam)-Fe(NO)Cl]^0	*cis*-[(cyclam)-Fe(NO)I]$^+$I (**2**)	[L′Fe(NO)(NO_2)$_2$]$^+$-(ClO_4)
S_t	$^3/_2$	$^1/_2$	0	0	$^3/_2$	0
$D_{3/2}$, cm^{-1}	+13.6				+12.6	
$E/D_{3/2}$	0				<0.01	
g^{eff}	4.0,2.0	2.052, 2.015, 1.970			3.99, 1.98	
$A_x^{eff}/g_N\beta_N$,T[a]	−21.3	−23.4			−20.0	
$A_y^{eff}/g_N\beta_N$,T	−20.8	−13.7			−24.8	
$A_z^{eff}/g_N\beta_N$,T	−25.4	11.9			−23.4	
$A_{Fe(III),x}/g_N\beta_N$,T[b]	−15.2	−14.0[d]			−14.3	
$A_{Fe(III),y}/g_N\beta_N$,T[b]	−14.9	−8.2[d]			−17.7	
$A_{Fe(III),z}/g_N\beta_N$,T[b]	−18.2	+7.1[d]			−16.7	
$A_{iso}/g_N\beta_N$[b,c]	−16.1	−5.0[d]			−16.2	
δ, mm s^{-1}	0.62	0.27	0.04	0.27	0.64	0.03
ΔE_Q, mm s^{-1}	−1.28	+1.26	+2.05	+0.77	−1.78	+1.37
η	0.2	<0.1	0	0.5	0.4	0.1
Γ, mm s^{-1}	0.42	0.33	0.27	0.42	0.39	0.3

[a] Hyperfine coupling tensor in the system of the total molecular spins $S_t = {}^3/_2$ and $^1/_2$, respectively. [b] Hyperfine coupling tensor with respect to local iron spin. [c] $A_{iso} = {}^1/_3\mathrm{tr}(A_{Fe(III)})$. [d] Values with respect to a local iron spin of $S = {}^3/_2$ (intermediate spin).

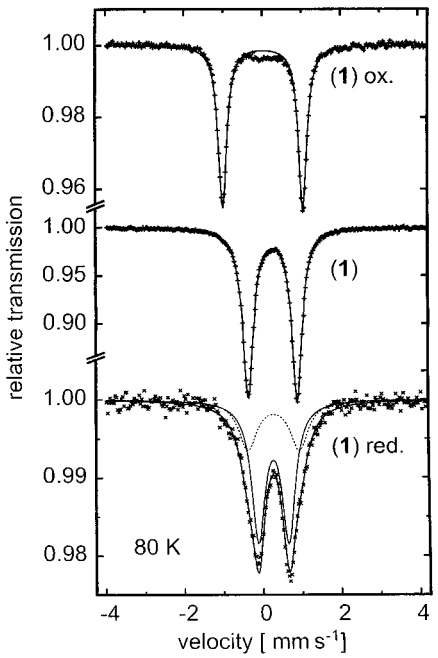

Figure 8. Zero-field Mössbauer spectra at 80 K of solid **1** (middle): the one-electron oxidized form of **1** (top) in frozen CH_3CN (0.10 M [(n-Bu)$_4$N]PF_6) and of the one-electron reduced (∼70%) form of **1** (bottom) where the minor spectrum (···) is that of **1**.

(N_3)$_2$]$^+$ ($S = {}^5/_2$) and *trans*-[(cyclam)Fe^{III}(N_3)$_2$]$^+$ ($S = {}^1/_2$).[15] It is remarkable that the observed $\Delta\delta$ of 0.37 mm s^{-1} for the pair of complexes **2** and **1** is exactly between the corresponding differences for similar ferric and ferrous complexes. The magnetic properties given below, however, show that it is not the valence state of iron that is ambiguous in this case but rather the spin states are unusual. The iron can be consistently described as Fe(III) for **1** and **2**.

To measure the Mössbauer spectra of the one-electron oxidized and one-electron reduced forms of **1** we have used 35% ^{57}Fe isotopically enriched **1** and electrochemically generated these forms in acetonitrile solution (0.10 M [(n-Bu)$_4$N]-PF_6).

Figure 8 (top) shows the zero-field spectrum of *trans*-[(cyclam)Fe(NO)Cl]$^{2+}$ at 80 K. A single quadrupole doublet with an isomer shift of 0.04 mm s^{-1} and a quadrupole splitting of 2.05 mm s^{-1} is observed. Thus one-electron oxidation of **1** decreases the isomer shift by 0.23 mm s^{-1}. It is again instructive to compare this shift with the corresponding shift of 0.26 mm s^{-1} observed for the complexes *trans*-[(cyclam)Fe^{II}(N_3)$_2$] ($S = 0$) and low-spin *trans*-[(cyclam)Fe^{III}(N_3)$_2$]$^+$ ($S = {}^1/_2$).[15] Thus one-electron oxidation of the {Fe−NO}^{7} ($S = {}^1/_2$) core in **1** to {Fe−NO}^{6} ($S = 0$) represents a metal-centered one-electron oxidation.

The small isomer shift of *trans*-[(cyclam)Fe(NO)Cl]$^{2+}$, an {Fe−NO}^{6} system, deserves a comment. We are aware of only one other report where even smaller isomer shifts of +0.04 and −0.02 mm s^{-1} at 80 K have been reported for two five-coordinate, structurally characterized {Fe−NO}^{6} ($S = 0$) species, namely [Fe(HL)NO](NO_3) and [Fe(*n*-C_3H_7)$_2$Q(NO)], where H_3L is 2,4-pentanediane-bis(*S*-methylisothiosemicarbazone) and (*n*-C_3H_7)$_2$Q is the dianion nitromalonedialdehyde-bis(*S*-propylisothiosemicarbazonate).[29] The authors discuss the electronic structure of these compounds as intermediate between Fe^{IV}(NO)$^{1-}$ (Fe^{IV} $S = 1$ and NO$^-$ $S = 1$) and Fe^{III}(NO) (Fe^{III} low spin $S = {}^1/_2$ and coordinated neutral NO $S = {}^1/_2$).

Figure 8 (bottom) shows the zero-field Mössbauer spectrum of an ∼70% reduced sample of **1** which contains ∼30% of the starting material, the Mössbauer spectrum of which is known. Two quadrupole doublets in the ratio 68:32 are observed. The most salient feature of this spectrum is the fact that the isomer shift at 80 K of *trans*-[(cyclam)Fe(NO)Cl]^0 at 0.27 mm s^{-1} is within experimental error *identical* with that of **1**. Only the quadrupole splitting parameters differ significantly; $|\Delta E_Q|$ at 80 K is 1.26 mm s^{-1} for **1** but only 0.77 mm s^{-1} for the reduced form which contains an {Fe−NO}^{8} moiety. We consider this result remarkable because it proves that the additional electron in the reduced complex does not change the s-electron density at the iron nucleus and must, therefore, occupy a π^* orbital of the nitrosyl ligand which is not involved in nitrogen-to-iron bonding. Thus in contrast to the above metal-centered one-electron oxidation of **1** the corresponding reduction is ligand-centered.

Oxidation and reduction derivatives of the $S = {}^3/_2$ system could not be studied directly by using the *cis*-cyclam complex **2** because of its instability in solution. However, the oxidized {Fe−NO}^{6} complex [L′Fe(NO)(ONO)(NO_2)]$^+$ ($S = 0$) was prepared as described above. The zero-field Mössbauer spectrum of the solid material (Figure S2, Supporting Information) shows a pure, well-resolved quadrupole doublet. The isomer shift is found at 0.02 mm s^{-1} (0.03 mm s^{-1} at 4.2 K) which is 0.6 mm

(29) Gerbeleu, N. V.; Arion, V. B.; Simonov, Yu. A.; Zavodnik, V. E.; Stavrov, S. S.; Turta, K. I.; Gradinaru, D. I.; Birca, M. S.; Pasynskii, A. A.; Ellert, O. *Inorg. Chim. Acta* **1992**, *202*, 173.

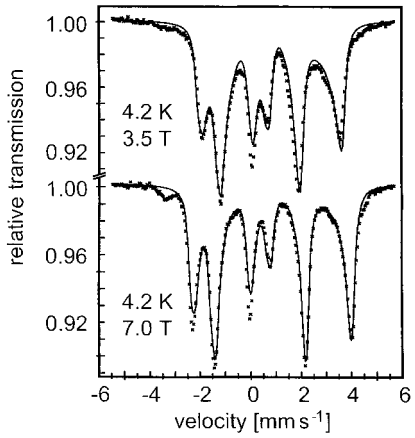

Figure 9. Applied-field Mössbauer spectra of solid $[LFe(NO)(N_3)_2]$ at 4.2 K. Simulation parameters are given in Table 5.

s^{-1} below the value found for the {Fe−NO}^{7} species $[LFe(NO)(N_3)_2]$. The quadrupole splitting is 1.37 mm s^{-1} (temperature-independent). A magnetically perturbed measurement performed at 4.2 K (see below) reveals a change of sign of V_{zz} of the electric field gradient on going from $[L'Fe(NO)(ONO)(NO_2)]^+$ where it is positive to $[LFe(NO)(N_3)_2]$ where it is negative.

For the purpose of an educated comparison we have also recorded the zero-field Mössbauer spectra at 80 K of an octahedral ferrous species, $[Fe^{II}(P(OC_2H_5)_3)_5Br]^+$ ($S = 0$), and its five-coordinate, trigonal bipyramidal nitrosyl iron complex $[Fe(NO)(P(OC_2H_5)_3)_4]BPh_4$ ($S = 0$) of the {Fe−NO}^{8} type which probably contains a linear {Fe−NO}^{8} moiety[25] and a ν(NO) stretching frequency at 1734 cm^{-1}. The first of these complexes displays a symmetrical quadrupole doublet at 0.15 mm s^{-1} and a quadrupole splitting of 0.76 mm s^{-1}, whereas for the nitrosyl complex these parameters are −0.02 and 1.85 mm s^{-1} (Figure S3, Supporting Information). The shift of ∼0.2 mm s^{-1} of the isomer shift on going from a low-spin ferrous species to the corresponding nitrosyl iron {Fe−NO}^{8} species indicates to us that the iron ion is more reduced in the latter than in the former. Thus the electronic structure of $[Fe(NO)(P(OC_2H_5)_3)_4]BPh_4$ can be described as $Fe^0(NO^+)$ (which we prefer) or $Fe^I(NO^*)$ (Fe^I $S = {}^1/_2$, NO^- $S = {}^1/_2$). A description as $Fe^{II}(NO^-)$ (Fe^{II} $S = 0$, NO^- $S = 0$) is not appropriate. Note that this difference of isomer shifts on going from the intermediate spin of the Fe(III) ion ($S = {}^3/_2$) in [*trans*-(cyclam)$_2${Fe^{III}-(μ-N)Fe^{IV}}$(N_3)_2]^{2+}$ ($S_t = {}^1/_2$)[15] to *trans*-[(cyclam)Fe(NO)Cl]$^+$ ($S = {}^1/_2$) is only 0.07 mm s^{-1}, which indicates to us that the iron ions in both complexes have the same oxidation state and similar d^n electron configuration, namely intermediate spin ferric.

(b) Applied Field Mössbauer Spectra. Application of 1.5−7 T magnetic fields at liquid helium temperatures resolves the magnetic hyperfine splitting of solid **2** and $[LFe(NO)(N_3)_2]$ as is shown in Figures 9 and 10. The spectra were readily simulated for an $S = {}^3/_2$ spin system in the limit of fast relaxation. These Spin-Hamiltonian simulations yield hyperfine coupling tensors, the sign and magnitude of the quadrupole splitting, and the isomer shift with the other parameters (g, D, E/D) set to the values determined from EPR and magnetic susceptibility measurements. Details of the Spin-Hamiltonian analyses are described in ref 15; the parameters are given in Table 5.

In strong applied field (7 T) at 4.2 K both complexes show an asymmetric magnetic six-line pattern with overall splittings of 6.2 mm s^{-1} for $[LFe(NO)(N_3)_2]$ and 7.5 mm s^{-1} for **2**. The corresponding internal fields originate from induced spin expectation values of the electronic spin ground-state Kramers doublet $|{}^3/_2, \pm{}^1/_2\rangle$ which is exclusively populated at 4.2 K due

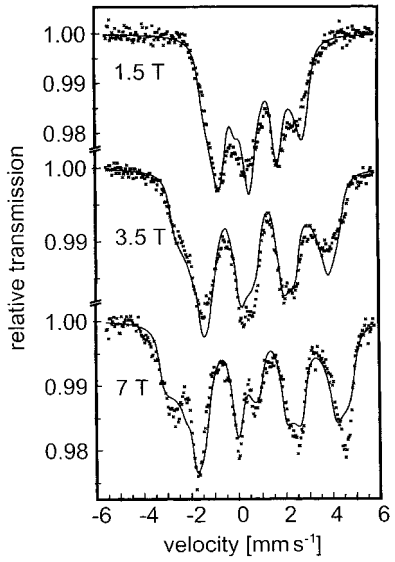

Figure 10. Applied-field Mössbauer spectra of solid **2** at 4.2 K. Simulation parameters are given in Table 5.

to the large zero-field splitting (ZFS) ($2D_{3/2}/k > 30$ K). Since fast spin relaxation prevails in the spectra of $[LFe(NO)(N_3)_2]$ and **2**, it is the thermal average $\langle\vec{S}\rangle_T$ of the spin expectation value which determines the internal field $\vec{B}^{int} = \bar{A}^{eff}\langle\vec{S}\rangle_T$. In the fast relaxation regime the internal field depends on the applied field because $\langle\vec{S}\rangle_T$ varies for variant Zeeman splitting of the ground-state Kramers doublet. This behavior, however, is modified by the mixing of magnetic sublevels due to competing ZFS and Zeeman interaction which, hence, yields a measure of the ZFS. On the basis of these considerations the magnetic Mössbauer spectra of $[LFe(NO)(N_3)_2]$ and **2** are readily consistent with the large ZFS parameters $D_{3/2}$ determined from the magnetic susceptibility data. In particular, the positive sign of $D_{3/2}$ is unambiguous from the magnetic anisotropy observed in the spectra.

According to the axial symmetry of the ZFS interaction as determined by the EPR spectra of both compounds ($E/D = 0$), the ground-state Kramers doublet $|{}^3/_2, +{}^1/_2\rangle$ shows an "easy-plane" of magnetization. This means for the molecules in a powder sample that the spin expectation values and the resulting internal fields $\vec{B}^{int}$ are much stronger for applied fields in the molecular x/y-direction (of the ZF-interaction) than for those close to the z-direction. Therefore, the x- and y-components of the **A**-tensor are better determined by the simulations than the z-component. The values of A_x^{eff} and A_y^{eff} are found to be very close to each other for both compounds, whereas the fits of the asymmetry of the hyperfine lines and the field dependence of the magnetic splittings could be improved if A_z^{eff} was allowed to take larger values than A_x^{eff}/A_y^{eff}. In any case, the signs of the $\bar{A}^{eff}$ components are negative for both $S = {}^3/_2$ complexes.

For magnetic Mössbauer spectra with strong internal fields and dominating nuclear Zeeman interaction the quadrupole interaction is determined in first order only by the components of the electric field gradients (efg) tensor that are oriented along the internal field. Since the internal fields for $[LFe(NO)(N_3)_2]$ are predominantly in the x/y-plane only the V_{xx} and V_{yy} components of the efg-tensor are effective for the appearance of the spectra. Since these components have the *opposite* sign than the main component V_{zz} and the *apparent* quadrupole shifts in the magnetic hyperfine pattern are positive, V_{zz} is in fact *negative* which is consistent with other examples of {Fe−NO}^{7} ($S = {}^3/_2$) systems (Table 1). For both complexes the asymmetry parameter of the efg is found to be small ($\eta \approx 0.2-0.4$). For

[LFe(NO)$(N_3)_2$] we could not detect significant orientational differences of the principal axis systems (pas) of the efg and ZF interaction, except for a minor rotation of $V_{z'z'}$ off from the *z*-axis of the ZFS. Systematic searches yield an Euler-rotation (β,*y*′) of the efg with $\beta = 18°$. For **2** the efg rotations appear to be more complex. We found sizable Euler angles $\alpha = 51°$, $\beta = 21°$, $\gamma = 59°$ for the three rotations with respect to the axes *z*, *y*′, *z*″. However, most significant is again $\beta = 21°$ which means again that the main component $V_{z'z'}$ is oriented away from the *z*-axis by about 20°, similar as for [LFe(NO)$(N_3)_2$]. We mention that rotations around the *z*-axis are less important because of the high, almost axial symmetry of the ZFS and, similarly, the **A**-tensor.

The negative **A**-tensor components of [LFe(NO)$(N_3)_2$] and **2** support the suggested spin-coupling model for the {Fe−NO}^{7} ($S = {}^3/_2$) unit which is based on the assignments of high-spin Fe^{III} ($S = {}^5/_2$) and NO^- ($S = 1$). In this model the ground state $S = {}^3/_2$ of the molecule results from strong antiferromagnetic coupling between the two local spin systems. Since then the spin of Fe^{III} is parallel to the system spin, the A^{eff}-tensor in the coupled system has the same (negative) sign as the intrinsic tensor $A_{Fe(III)}$. (This is at least true for the isotropic part A_{iso}.) From an application of the Wigner−Eckart theorem one deduces the relation of intrinsic and coupled **A**-tensor components: $A_{Fe(III)} = +{}^5/_7 A^{eff}$. The resulting intrinsic values of $\bar{A}_{Fe(III)}$ are given in Table 5. The isotropic parts $A_{iso}/g_N\beta_N = -16$ T for both complexes are lower than that of typical "ionic" Fe^{III} moieties (−20 to −22 T)[30] but are quite consistent with that found for Fe^{III} in iron−sulfur clusters (≈ -16.5 T)[31] which also experience significantly covalent bonds.

The anisotropy of the **A**-tensor of [LFe(NO)$(N_3)_2$] was recently explained by covalent delocalization of *some* of the d-orbitals.[3] Anisotropic covalency of d-orbitals is also the reason for the large quadrupole splittings found in some cases of Fe^{III} compounds, which in the "ionic" limit would show no or only small splittings due to the symmetry of the S-state ion. For instance, similar large values such as those of [LFe(NO)$(N_3)_2$] and **2** or even larger ones are reported for various compounds with the (μ-oxo)diiron(III) unit.[32]

The magnetic Mössbauer spectrum of **1** measured at 150 K with 7 T applied field as shown in Figure 11 (top) unambiguously reveals a positive sign of the efg main-component V_{zz}, and a vanishing asymmetry parameter $\eta = 0$ (error range +0.1). At liquid helium temperatures the applied-field spectra recorded at 1, 3.5, 5, and 7 T show only rather broad lines and a relatively weak overall splitting, in accordance with the low total spin state. In addition, the weak magnetic splitting indicates also a small isotropic part of the hyperfine coupling tensor. The asymmetry of the spectra shown in Figure 11, in conjunction with a large quadrupole splitting, is typical of substantial anisotropy of the hyperfine tensor. Spin-Hamiltonian simulations which were performed with $S = {}^1/_2$, *g* values taken from EPR, and the **g** matrix elements all set positive, yield for **1** a coupling tensor $\mathbf{A}^{eff}/g_N\beta_N = (-23.4, -13.7, +11.9)$ T.

When different orientations of efg and $\bar{A}_{1/2}$ tensor principal axes systems were allowed, the fits could be significantly improved only by an Euler rotation of the efg around the *y*-axis by a small angle $\beta = 6°$. Interestingly, this angle resembles the tilting angle $\theta = 7.6°$ that was found between the normal of the cyclam(nitrogen) plane and the axis through Fe and the average of N and O atom positions.

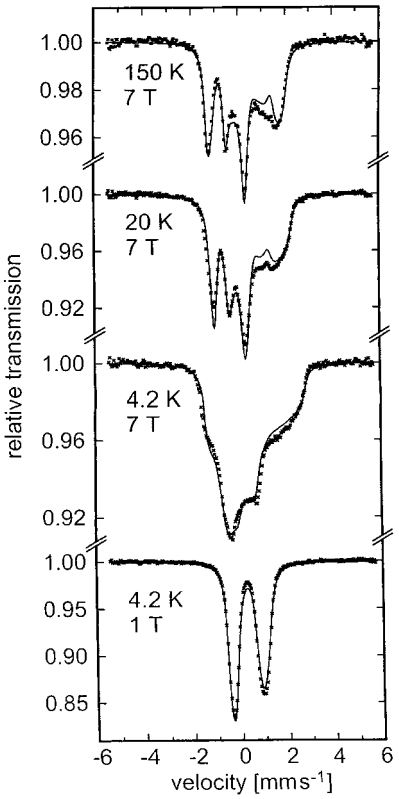

Figure 11. Variable-temperature, variable-field Mössbauer spectra of **1**, *trans*-[(cyclam)Fe(NO)Cl]$^+$ (35% ^{57}Fe enriched), in CH_3CN (0.10 M [(n-Bu)$_4$N]PF_6). Simulation parameters are given in Table 5.

The isotropic part of the $\mathbf{A}^{eff}$ tensor obtained for **1** is clearly negative, ${}^1/_3\mathrm{tr}(\mathbf{A})/g_N\beta_N = -8.4$ T. This observation rules out the description of **1** as an antiferromagnetically coupled low-spin ferric ion ($S = {}^1/_2$) and an NO^- ($S = 1$) ligand, since in this case the apparent $\mathbf{A}^{eff}$ tensor in the coupled spin system would exhibit a positive isotropic part for a negative intrinsic value of iron. Even if this argument might be obscured by undefined signs of the *g* values, which can be a problem for low-spin Fe^{III} (the Mössbauer spectra are sensitive only for the product $g_i \cdot A_i$),[33] the magnetic spectra of **1** are not consistent with the interpretation of low-spin Fe^{III} at all for the following reasons: (i) The efg does not match: The small anisotropy of the *g* values obtained from the EPR spectra would clearly mean for a low-spin Fe^{III} interpretation that the electron−hole in the $(t_{2g})^5$ configuration has to reside in an energetically well isolated d-orbital which is virtually not mixed by spin−orbit coupling ($\sum g_i^2 = 12.15$). For instance, in the crystal-field model developed by Griffith[34] and Taylor,[35] the best description of **1** would be obtained with large axial and rhombic orbital splittings of $\Delta/\lambda = 96$ and $V/\lambda = \pm 46$, which corresponds to a situation of a practically pure configuration $(d_{xy}, d_{xz})^4(d_{yz})^1$ (or, equivalently, $(d_{xy}, d_{yz})^4(d_{xz})^1$). The resulting charge anisotropy of the valence electrons caused by the electron−hole in a single "pancake"-shaped t_{2g} orbital would lead to a strong *negative* valence contribution to the main component of the efg[30] (either in the *x*- or the *y*-direction), which is in contradiction to the

(30) Srivastava, J. K.; Bhargara, S. C.; Iyengar, P. K.; Thosar, B. V. In *Advances in Mössbauer Spectroscopy*; Thosar, B. V., Iyengar, P. K., Eds.; Elsevier: New York, 1983; pp 1−121.

(31) Münck, E. *Methods Enzymol.* **1978**, *54*, 346. (b) Huynh, B. H.; Kent, T. A. In *Advances in Mössbauer Spectroscopy*; Thosar, B. V., Iyengar, P. K., Eds.; Elsevier: New York, 1983; pp 490−560.

(32) Rodriguez, J. H.; Xia, Y.-M.; Debrunner, P. G.; Chaudhuri, P.; Wieghardt, K. *J. Am. Chem. Soc.* **1996**, *118*, 7542−7550 and references therein.

(33) Huynh, B. H.; Emptage, M. H.; Münck, E. *Biochim. Biophys. Acta* **1978**, *534*, 295−306.

(34) Griffith, J. S. *Proc. R. Soc. London, A* **1956**, *235*, 23−36.

(35) Taylor, C. P. S. *Biochim. Biophys. Acta* **1977**, *491*, 137.

experimental observation. Even if covalency and lattice contributions significantly influence the actual values of the efg components, it is difficult to envisage a reversal of the sign of $V_{z'z'}$, particulary in this case of a strong axially symmetric efg. (ii) The symmetry of the magnetic hyperfine coupling tensor $\mathbf{A}^{\text{eff}}$ as can be derived from the t_{2g}-hole description of **1** is also not consistent with the experiment: The orbital and spin-dipolar contributions to **A** in this model[33,36] yield the largest, negative component of **A** in the direction of the efg main component, whereas in the simulations of the spectra the A^{eff} component along the efg *z*-direction was found to be the weakest (and positive).

These arguments led us to consider the alternative description of **1**, not as a low-spin Fe^{III} complex but as an antiferromagnetically coupled system of *intermediate*-spin ferric ion ($S = {}^3/_2$) and an NO^- ($S = 1$). Since in this picture iron has the major local spin, the sign of the isotropic part $A_{\text{iso}}{}^{\text{eff}}$ with respect to the system spin $S_t = {}^1/_2$ is the same as that of the (negative) intrinsic value. The value of the isotropic part turns out to be rather weak in this model (${}^1/_3\text{tr}(\mathbf{A}_{\text{Fe(III)},S=3/2}) = -5$ T), when the experimental value for the system spin is converted according to the spin-projection formula $\mathbf{A}_{\text{Fe(III)},S=3/2} = +{}^3/_5\,\mathbf{A}^{\text{eff}}$. However, this does not contradict the basic assumption of intermediate spin Fe^{III}, because it is clear that spin-dipolar contributions and covalent orbital delocalizations cannot be neglected for a nitrosyl complex.

Iron(III) intermediate spin states were first reported for five-coordinate iron porphyrinates with square-pyramidal geometry;[37] but other examples with salen and dithiocarbamate and other ligands are also described in detail.[38−40] The large positive quadrupole splitting ($\approx$+3 mm s^{-1}, $\eta \approx 0$) was recognized as a characteristic feature of intermediate-spin ferric porphyrinates.[41] Detailed analyses of EPR and Mössbauer spectra showed the presence of a highly anisotropic hyperfine tensor with large, negative components in *x*/*y*-directions and weak, positive *z*-components. Both features, the positive, axial quadrupole interaction and the anisotropic magnetic hyperfine tensor, are very similar to what we found for **1**. In the theoretical model developed by Maltempo[42] the "spin-Hamiltonian" parameters[43] are derived by mixing of close lying $^4A_2$ and $^6A_1$ orbital singlet states. Square-planar geometry was taken as the starting point for the description of the spin-quartet ground state, according to the assumption that the antibonding $d_{x^2-y^2}$ orbital is too high in energy above the d_{z^2} and the $d\pi$ orbitals to be populated. The resulting ground-state configuration is basically $(d_{xy})^2(d_{xz})^1(d_{yz})1(d_{z^2})^1$.

High-field Mössbauer measurements (7 T, 4.2 K) of the {Fe−NO}^{8} and the {Fe−NO}^{6} species derived from **1** by electrochemical reduction and oxidation, respectively, reveal an $S = 0$ ground state for both complexes, namely *trans*-[(cyclam)Fe(NO)(Cl)]^0 and *trans*-[(cyclam)Fe(NO)(Cl)]$^{2+}$. Also, for [L′Fe(NO)(ONO)(NO$_2$)]$^+$, an {Fe−NO}^{6} species, a diamagnetic ground state has been established. We assume that the $S = 0$ ground state of these complexes owes its origin to strong intramolecular spin couplings (see below). The magnetic Mössbauer spectra (Figure S4) were simulated by using the isomer shifts and the electric quadrupole splittings from the respective zero-field spectra. All species, namely the {Fe−NO}^{6} and the {Fe−NO}^{8} derivatives of **1** and [L′Fe(NO)(ONO)(NO$_2$)]$^+$, possess a positive sign of the quadrupole splitting and high axial symmetry of the efg with $\eta \approx 0$. The low isomer shift and large, positive quadrupole splitting with $\eta \approx 0$ of the two present {Fe−NO}^{6} species are consistent with those observed for Werner-type octahedral low-spin Fe^{IV} complexes.[15] The axial efg can be rationalized in a ligand field model for the spin−orbit interaction of distorted octahedral $(t_{2g})^4$ complexes. In this model the valence contribution to the efg originates from two electron holes in the t_{2g} subshell which is positive for a $(d_{xy})^2(d_{xz})^1(d_{yz})^1$ ground-state configuration of Fe^{IV}.[44−47] Thus the electronic structures of *trans*-[(cyclam)Fe(NO)Cl]$^{2+}$ and [L′Fe(NO)(ONO)(NO$_2$)]$^+$, both of which are of the {Fe−NO}^{6} ($S = 0$) type, can be described as low-spin Fe^{IV} ($S = 1$) coupled antiferromagnetically to an NO^- ($S = 1$) ligand.

Discussion

Rodriguez et al.[3] have recently reported a detailed Mössbauer study and density functional theory calculation on the nitrosyl derivatives of deoxyhemerythrin which contains a high-spin ferrous site with isomer shift and quadrupole splitting at 1.21 and +2.66 mm s^{-1}, respectively, and a nitrosyl iron site {Fe−NO}^{7} ($S = {}^3/_2$) with 0.68 and +0.61 mm s^{-1}, respectively. While the isomer shift for the former was considered to be normal (typical) for an octahedral ferrous ion in an oxygen/nitrogen donor environment, the latter value has been considered "unusual" or not typical (in fact enhanced) with respect to a normal high-spin ferric ion or, conversely, reduced with respect to a high-spin ferrous ion. They concluded that an isomer shift of 0.68 mm s^{-1} is intermediate between high-spin ferrous and ferric and does not allow an oxidation state assignment.

In contrast to this interpretation we would like to point out that the isomer shift is only considered to be unusual because there are but few high-spin ferric complexes reported to date with such large isomer shift. For example, Lippard et al.[48] have structurally characterized a (μ-1,2-peroxo)diiron(III) complex

(36) Oosterhuis, W. T.; Lang, G. *Phys. Rev.* **1969**, *178*, 439−456. (b) Lang, G.; Marshall, W. *Proc. Phys. Soc.* **1966**, *87*, 3−34. (c) Safo, M. K.; Gupta, G. P.; Walker, F. A.; Scheidt, W. R. *J. Am. Chem. Soc.* **1991**, *113*, 5497−5510. (d) Walker, F. A.; Huynh, B. H.; Scheidt, W. R.; Osvath, S. R. *J. Am. Chem. Soc.* **1986**, *108*, 5288−5297.

(37) Debrunner, P. G. *Mössbauer Spectroscopy of Iron Porphyrins*; Debrunner, P. G., Ed.; VCH: Weinheim, 1989; Vol. III, pp 137−234. (b) Scheidt, W. R.; Osvath, S. R.; Lee, Y. J.; Reed, C. A.; Shaevitz, B.; Gupta, G. P. *Inorg. Chem.* **1989**, *28*, 1591−1595.

(38) Niarchos, D.; Kostikas, A.; Simopoulos, A.; Coucouvanis, D.; Piltingsrud, D.; Coffman, R. E. *J. Chem. Phys.* **1978**, *69*, 4411−4418. (b) Ganguli, P.; Marathe, V. R.; Mitra, S. *Inorg. Chem.* **1975**, *14*, 970−973. (c) Ganguli, P.; Hasselbach, K. M. *Z. Naturforsch.* **1979**, *34a*, 1500−1506. (d) Wells, F. V.; McCann, S. W.; Wickman, H. H.; Kessel, S. L.; Hendrickson, D. N.; Feltham, R. D. *Inorg. Chem.* **1982**, *21*, 2306−2311. (e) Kuang, X.-Y.; Morgenstern, I.; Rodriguez, M.-C. *Phys. Rev. B* **1993**, *48*, 6676−6679. (f) Kuang, X.-Y.; Morgenstern-Badarau, I. *Phys. Status Solidi B* **1995**, *191*, 395−400.

(39) Kostka, K. L.; Fox, B. G.; Hendrich, M. P.; Collins, T. J.; Rickard, C. E. F.; Wright, L. J.; Münck, E. *J. Am. Chem. Soc.* **1993**, *115*, 6746.

(40) Kentel, H.; Käpplinger, I.; Jäger, E.-G.; Grodzicki, M.; Schünemann, V.; Trautwein, A. X. *Inorg. Chem.* **1999**, *38*, 2320. (b) Koch, S.; Holm, R. H.; Frankel, R. B. *J. Am. Chem. Soc.* **1975**, *97*, 6714. (c) Gupta, G.; Lang, G.; Reed, C. A.; Shelly, K.; Scheidt, W. R. *J. Chem. Phys.* **1987**, *86*, 5288.

(41) Dolphin, D. H.; Sams, J. R.; Tsin, T. B. *Inorg. Chem.* **1977**, *16*, 711.

(42) Maltempo, M. M. *J. Chem. Phys.* **1974**, *61*, 2540−2547. (b) Maltempo, M. M.; Moss, T. H. *Q. Rev. Biophys.* **1976**, *9*, 181−215.

(43) Neese, F.; Solomon, E. I. *Inorg. Chem.* **1998**, *37*, 6568−6582.

(44) Moss, T.; Ehrenberg, A.; Bearden, A. J. *Biochemistry* **1969**, *8*, 4159−4162. (b) Schulz, C. E.; Rutter, R.; Sage, J. T.; Debrunner, P. G.; Hager, L. P. *Biochemistry* **1984**, *23*, 4743−4754. (c) Mandon, D.; Weiss, R.; Jayaraj, K.; Gold, A.; Terner, J.; Bill, E.; Trautwein, A. X. *Inorg. Chem.* **1992**, *31*, 4404−4409 and references therein.

(45) (a) Jayaraj, K.; Gold, A.; Austin, R. N.; Ball, L. M.; Terner, J.; Mandon, D.; Weiss, R.; Fischer, J.; DeCian, A.; Bill, E.; Müther, M.; Schünemann, V.; Trautwein, A. X. *Inorg. Chem.* **1997**, *36*, 4555−4566. (b) Jayaraj, K.; Gold, A.; Austin, R. N.; Mandon, D.; Weiss, R.; Terner, J.; Bill, E.; Müther, M.; Trautwein, A. X. *J. Am. Chem. Soc.* **1995**, *117*, 9079−9080 and references therein.

(46) Oosterhuis, W. T.; Lang, G. *J. Chem. Phys.* **1973**, *58*, 4757−4765.

(47) Paulsen, H.; Müther, M.; Grodzicki, M.; Trautwein, A. X.; Bill, E. *Bull. Soc. Chim. Fr.* **1996**, *133*, 703−710.

(48) Kim, K.; Lippard, S. J. *J. Am. Chem. Soc.* **1996**, *118*, 4914.

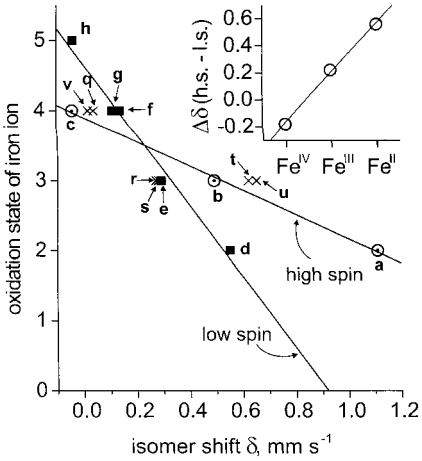

Figure 12. Plot of the formal oxidation state of the iron ions in complexes vs the isomer shift, δ: *cis*-[(cyclam)$Fe^{II}(N_3)_2$] (**a**); *cis*-[(cyclam)$Fe^{III}(N_3)_2]^+$ (**b**); $[Et_4N][Fe^{IV}Cl(\eta^4\text{-MAC*})]$ (**c**); *trans*-[(cyclam)$Fe^{II}(N_3)_2$] (**d**); *trans*-[(cyclam)$Fe^{III}(N_3)_2]^+$ (**e**); [(cyclam)(N_3)-Fe^{III}═N═$Fe^{IV}(N_3)$(cyclam)]$^{2+}$ $S = {}^3/_2$ (**g**); [(cyclam)$(N_3)Fe^{III}$═N═Fe^{IV}-(N_3)(cyclam)]$^{2+}$ $S = {}^1/_2$ (**f**); *trans*-[(cyclam)$Fe^{V}(N)(N_3)]^+$ (**h**); *trans*-[(cyclam)Fe(NO)Cl]$^{2+}$ (**q**); *trans*-[(cyclam)Fe(NO)Cl]$^+$ (**r**); *trans*-[(cyclam)Fe(NO)Cl]^0 (**s**); *cis*-[(cyclam)Fe(NO)I]I (**t**), [LFe(NO)$(N_3)_2$] (**u**), and [LFe(NO)(ONO)$(NO_2)]^+$ (**v**). The inset shows the isomer shift difference, $\Delta\delta$, between high and low spin complexes in a similar ligand environment at a given common oxidation state (Fe^{IV}, Fe^{III}, or Fe^{II}).

that contains two octahedral high-spin ferric ions (N_3O_3Fe) and exhibits in frozen toluene solution at 4.2 K a Mössbauer spectrum consisting of a symmetrical doublet with isomer shift and quadrupole splitting of $\delta = 0.66$ mm s^{-1} and $\Delta E_Q = 1.40$ mm s^{-1} ($\Gamma = 0.15$ mm s^{-1}). This isomer shift corresponds exactly to the value reported for the peroxodiferric intermediate of methane monooxygenase.[49] Since the oxidation level of the O_2^{n-} bridge is unequivocally peroxide (O_2^{2-}), the assignment of a +III oxidation state for both iron ions is also unequivocal. The $Fe-O_{peroxo}$ bond is relatively short and displays covalent character. It resembles in this respect the situation in nitrosyliron or nitridoiron complexes.

In the following we attempt to correlate in a more general fashion Mössbauer isomer shifts with formal oxidation states of a given iron ion or, more to the point, with the d^n electron configuration of the central iron ion in a series of structurally very similar, preferably octahedral, complexes. In Figure 12 we have plotted the isomer shifts (at 4.2 K) of three *high-spin* configured complexes, namely *cis*-[(cyclam)$Fe^{II}(N_3)_2$] ($S = 2$),[15] *cis*-[(cyclam)$Fe^{III}(N_3)_2]^+$ ($S = {}^5/_2$),[15] and $[Et_4N][Fe^{IV}Cl(\eta^4$-MAC*)] ($S = 2$)[39] which we label **a**, **b**, and **c**, respectively. $H_4[\eta^4$-MAC*] is the tetradentate ligand 1,3,8,11-tetraaza-13,13-diethyl-2,2,5,5,7,7,10,10-octamethyl-3,6,9,12,14-pentaoxocyclotetradecane which is coordinated to an Fe^{IV} ion very much like cyclam except that the four nitrogen donor atoms are amides rather than amines in cyclam. The monoanionic complex is five-coordinate (FeN_4Cl). These three complexes are for all our purposes considered to be "isostructural". Their isomer shifts increase linearly with decreasing d^n configuration d^6, d^5, d^4. In other words, a constant shift of the isomer shift of 0.57 mm s^{-1} per one-electron change is observed for this series.

In a second series we correlate, as above, known *low-spin* iron complexes:[15] *trans*-[(cyclam)$Fe^{II}(N_3)_2$] ($S = 0$), *trans*-[(cyclam)$Fe^{III}(N_3)_2]^+$ ($S = {}^1/_2$),[15] and *trans*-[(cyclam)Fe^{V}(N)-$(N_3)]^+$ ($S = {}^3/_2$)[15] which are labeled **d**, **e**, and **h** in Figure 12. The oxidation state +IV is attained in two isomers of [(cyclam)-$(N_3)Fe^{III}$═N═$Fe^{IV}(N_3)$ (cyclam)]$^{2+}$ with either an $S_t = {}^3/_2$ or $S_t = {}^1/_2$ ground state. Both give rise to two quadrupole doublets (Fe^{III} ($S = {}^3/_2$ or $^1/_2$) and Fe^{IV} ($S = 1$)) for each complex; the isomer shift of both Fe^{IV} ($S = 1$) ions in the two isomers is nearly identical (labels **f** and **g** in Figure 12). Again the isomer shift increases linearly with decreasing oxidation number.[15] Interestingly, the change of isomer shift per one-electron change of d^n configuration is significantly smaller (only 0.19 mm s^{-1}) than that for the above high-spin complexes. Note that all low-spin complexes considered here have an octahedral FeN_6 coordination polyhedron; three contain the strong π donor ligand nitride which is bound to high-valent iron in a quite covalent fashion[50] but the other two do not.

Closer inspection of the two straight lines in Figure 12 reveals an interesting facet of this analysis. From the plot we can immediately see that a high-spin−low-spin crossover affects the isomer shift in a different fashion for each oxidation state (see the inset in Figure 12). A very large positive $\Delta\delta$ (high-low spin) of ~0.6 mm s^{-1} is observed for ferrous complexes; for ferric complexes this difference is still positive but smaller at +0.2 mm s^{-1}; on going to Fe^{IV} this difference becomes *negative*, −0.2 mm s^{-1}. Thus high-spin Fe^{IV} complexes have a smaller isomer shift than their low-spin counterparts, and for Fe^{III} and Fe^{II} high- and low-spin species it is the other way around.

Up to this point the above analysis should not be controversial. Obviously, the conclusions drawn rely heavily on the structural (and electronic) similarity of complexes chosen to generate a "series". We do not claim that these correlations hold for *all* iron complexes, e.g. $[Fe(CN)_6]^{3-/4-}$ complexes do not fit into the picture. Nevertheless, the concept has heuristic value as we attempt to show now.

{Fe−NO}^{7} ($S = {}^3/_2$). The complex [LFe(NO)$(N_3)_2$] has played a role model for nitrosyl iron complexes of the type {Fe−NO}^{7} ($S = {}^3/_2$). In-depth spectroscopic investigations[12] and calculations[3,12] have led to the conclusion that it can be best described as a high-spin ferric ion coupled to a NO^- ($S = 1$) yielding the observed $S = {}^3/_2$ ground state. At 4.2 K this complex has an isomer shift of +0.61 mm s^{-1}. Adding this data point to the plot in Figure 12 (labeled **t**) immediately shows that the isomer shift falls very close to the linear correlation of **a**, **b**, and **c** if an oxidation state of +III is assumed. In principle, the measured isomer shift could also be achieved by a low-spin ferrous ion ($S = 0$) using correlation **d**, **e**, **f**, **g**, and **h** but this necessitates the description of the {Fe−NO}^{7} ($S = {}^3/_2$) species as Fe^{II} ($S = 0$) coordinated to an NO^- radical which must then possess an $S = {}^3/_2$ configuration. This is of course not acceptable. Thus Mössbauer and Fe K-edge energy X-ray absorption spectroscopy (XAS) are fully in accord with a formalism where a high-spin ferric ion is antiferromagnetically coupled to an NO^- ($S = 1$) ligand. Exactly the same arguments hold for *cis*-[(cyclam)Fe(NO)I]I (data point **u** in Figure 12) and for all {Fe−NO}^{7} ($S = {}^3/_2$) species including the nitrosyl derivatives of non-heme proteins listed in Table 1.

{Fe−NO}^{7} ($S = {}^1/_2$). For complex **1** the isomer shift at 4.2 K has been determined to be 0.27 mm s^{-1}. The *trans*-cyclam ligand in octahedral ferric or ferrous complexes enforces in general a low-spin configuration. Recently a few cases have been reported where this trans configuration also stabilizes an

(49) Liu, K. E.; Valentine, A. M.; Qiu, D.; Edmonson, D. E.; Appelman, E. H.; Spiro, T. G.; Lippard, S. J. *J. Am. Chem. Soc.* **1995**, *117*, 4997. (b) Liu, K. E.; Valentine, A. M.; Wang, D.; Huynh, B. H.; Edmonson, D. E.; Salifoglou, A.; Lippard, S. J. *J. Am. Chem. Soc.* **1995**, *117*, 10174.

(50) Jüstel, T.; Müller, M.; Weyhermüller, T.; Kressl, C.; Bill, E.; Hildebrandt, P.; Lengen, M.; Grodzicki, M.; Trautwein, A. X.; Nuber, B.; Wieghardt, K. *Chem. Eur. J.* **1999**, *5*, 793.

intermediate spin state ($S = {}^3/_2$) at a ferric ion.[39,40] Using the two correlations in Figure 12 one could expect an isomer shift of 0.64 − 0.2 (difference h.s.-l.s.) = ∼0.4 mm s^{-1} for **1**, if we assume a high-spin ferric ion adopting a low-spin electron configuration ($S = {}^1/_2$). Clearly, data point **r** is off the line defined by **d**, **e**, **f**, **g**, and **h,** but not far. As pointed out above, the description of **1** as low-spin ferric ($S = {}^1/_2$) antiferromagnetically coupled to NO$^-$ ($S = 1$ or 0) is not compatible with the applied-field Mössbauer spectra, but the description with an intermediate spin ferric ion ($S = {}^3/_2$) antiferromagnetically coupled to an NO$^-$ ($S = 1$) ligand is.

Pure intermediate spin, five-coordinated complexes containing an $Fe^{III}N_4X$ coordination polyhedron have been reported to have isomer shifts of, for example, 0.18[40a] and 0.14 mm s^{-1},[39] which is somewhat smaller than the isomer shift of low-spin ferric complexes at ∼0.3 mm s^{-1}. We have shown[15] that the dinuclear complex [*trans*-(cyclam)$_2${Fe^{III}(μ-N)Fe^{IV}}(N$_3$)$_2$]$^{2+}$ ($S = {}^1/_2$) consists of an octahedral Fe^{IV} ion ($S = 1$) antiferromagnetically coupled to an *octahedral* intermediate spin ferric ion ($S = {}^3/_2$). Its Mössbauer spectrum at 80 K displays two quadrupole doublets with isomer shifts at 0.20 mm s^{-1} for the ferric and at 0.11 for the Fe^{IV} ion. The difference of isomer shifts on going from **2** to **1** can then be calculated as 0.64 − 0.2 (difference h.s.-l.s.) − 0.1 (difference l.s.-i.s.) = 0.3 mm s^{-1}, which nicely corresponds to the observed value for **1** of 0.27 mm s^{-1}. This estimate is further supported by the distinctly more negative isomer shift of a genuinely *low-spin* ferric {FeNO}^{7} ($S = {}^1/_2$) complex, namely the recently published compound [Fe(NO)(TC-515)].[51] The iron in this system which is five-coordinate but otherwise has rather similar ligands as **1** shows an isomer shift of only 0.06 mm s^{-1}. Thus Mössbauer spectroscopy gives a reasonable indication of the nature of the electronic structure of **1** as intermediate spin ferric ($S = {}^3/_2$) antiferromagnetically coupled to NO$^-$ ($S = 1$).

Recently, the Mössbauer spectra of two distinctly different crystalline forms of [Fe(TpivPP)(NO)(NO$_2$)]$^-$, a six-coordinate porphinato complex of {Fe−NO}^{7} ($S = {}^1/_2$) type, have been reported[52] which display distinctly different isomer shifts at 0.28 mm s^{-1} (4.2 K) for form 1 and 0.35 mm s^{-1} (4.2 K) for form 2. Applied-field Mössbauer spectra for these two forms have not been reported. It is tempting to assign the following electronic structures using the correlation in Figure 12: form 1, intermediate-spin ferric ($S = {}^3/_2$) coupled antiferromagnetically to NO$^-$ ($S = 1$), and form 2, low-spin ferric ($S = {}^1/_2$) coupled to NO$^-$ ($S = 1$). The authors have pointed out the similarity of the spectra of these model complexes to those measured for NO-bound hemes, e.g. of d_1 heme in diheme cytochrome *cd$_1$* nitrite reductase[53] and siroheme in the hemoprotein subunit of *E. coli* sulfite reductase.[54]

It appears that this model is also supported by the spin-density distribution on the Fe−NO fragment which was determined for nitrosylated hemes ($S = {}^1/_2$). Whereas the most sophisticated DFT calculations[55] still do not yield a very illustrative picture in this respect, the experimental data derived from EPR measurements[56,57] indicate that nearly 30% of the spin-density resides on the NO ligand in these complexes.

{Fe−NO}^{8} ($S = 0$). All diamagnetic complexes of this electronic structure reported to date are five-coordinate (trigonal bipyramidal) and possess a linear Fe−NO moiety. The coligands are invariably strong π-acceptors such as phosphines and phospites.[24−27] Their ν(NO) stretching frequencies are usually observed in the range 1730 ± 20 cm^{-1}. This class of complexes represents the least well characterized with regard to their electronic structure. Most authors imply a description involving a low-spin ferrous ion ($S = 0$) coordinated to an NO$^-$ ($S = 0$!). As we have shown for [Fe(NO)(P(OC$_2$H$_5$)$_3$)$_4$]BPh$_4$,[24] this {Fe−NO}^{8} ($S = 0$) species possesses a very small isomer shift of −0.02 mm s^{-1} at 80 K. We have argued above that such species are probably best described as Fe^0(NO$^+$) species because their "innocent" low-spin ferrous counterparts display a larger isomer shift at 0.15 mm s^{-1} for [Fe^{II}(P(OC$_2$H$_5$)$_3$)$_5$Br]$^+$ ($S = 0$).

Clearly, the electronic structure of reduced **1**, namely *trans*-[(cyclam)Fe(NO)Cl]^0 ($S = 0$), must be very different. We do not observe a ν(NO) band at ∼1730 cm^{-1} and its isomer shift has been determined to be 0.27 mm s^{-1} which is exactly the same value as that for **1**. Consequently, we propose an electronic structure invoking a low-spin ferric ion ($S = {}^1/_2$) antiferromagnetically coupled to the dianionic radical NO^{2-} ($S = {}^1/_2$). We expect the Fe−NO unit to be strongly bent (α(FeNO) ∼ 110−130°) and the N−O distance approaching that of a single bond with ν(NO) < 1500 cm^{-1}. More experimental spectroscopic data (Mössbauer and EXAFS) are called for on this interesting class of compounds; the above interpretation is admittedly speculative and rests entirely on the validity of the correlations in Figure 12.

{Fe−NO}^{6} ($S = 0$). Octahedral diamagnetic {Fe−NO}^{6} complexes are structurally well characterized, the earliest examples being *cis*-[Fe(NO)(S$_2$CN(C$_2$H$_5$)$_2$)$_2$(NO$_2$)][58] which exhibits a ν(NO) band at 1835 cm^{-1} and [Fe(ttp)(NO)(H$_2$O)]ClO$_4$[23] with a ν(NO) band at 1937 cm^{-1} (see also ref 21). The oxidized form of **1**, namely *trans*-[(cyclam)Fe(NO)Cl]$^{2+}$ ($S = 0$), and [L′Fe(NO)(ONO)(NO$_2$)]$^+$ fit well into this series. Their small isomer shifts clearly indicate to us that the one-electron oxidation of **1** is metal-centered in nature. These isomer shifts are in perfect agreement with other octahedral Fe^{IV} ($S = 1$) species such as the Fe^{IV} ions in [(cyclam)(N$_3$)Fe^{III}═N═Fe^{IV}(cyclam)(N$_3$)]$^{2+}$ ($S = {}^3/_2$ or ${}^1/_2$) for which an isomer shift of 0.11 mm s^{-1} has been determined.[15] On the basis of Figure 12 we can assign the following electronic structures to the {Fe−NO}^{6} species: a low-spin Fe^{IV} ($S = 1$) ion antiferromagnetically coupled to an NO$^-$ ($S = 1$) ligand. This has also been suggested by Gerbeleu et al.[29] for five-coordinate [Fe(HL)(NO)](NO$_3$) with an isomer shift of +0.04 mm s^{-1} at 80 K.

Conclusion

In this study we have shown that Mössbauer spectroscopy is a very useful spectroscopic tool for the elucidation of the actual electronic structure of a series of nitrosyliron complexes of the type {Fe−NO}^{6,7,8}. In particular, the isomer shift, δ, is a very sensitive parameter for the assignment of oxidation states of the iron ions (and, indirectly, of the nitrosyl ligand). We have shown that a consistent interpretation can be achieved by using an ionic bonding model for these complexes with defined metal oxidation states: Fe^{III} (low- and intermediate-spin electron configuration ($S = {}^1/_2$ and ${}^3/_2$), respectively, antiferromagneti-

(51) Franz, K. J.; Lippard, S. J. *J. Am. Chem. Soc.* **1999**, *121*, 10504.
(52) Nasri, H.; Ellison, M. K.; Chen, S.; Huynh, B. H.; Scheidt, W. R. *J. Am. Chem. Soc.* **1997**, *119*, 6274.
(53) Liu, M.-C.; Huynh, B. H.; Payne, W. J.; Peck, H. D., Jr.; Der Vartanian, D. V.; Le Gall, J. *Eur. J. Biochem.* **1987**, *169*, 253.
(54) Christner, J. A.; Münck, E.; Janick, P. A.; Siegel, L. M. *J. Biol. Chem.* **1983**, *258*, 11147.
(55) Rovira, C.; Kunc, K.; Hutter, J.; Ballone, P.; Parinello, M. *J. Phys. Chem. A* **1997**, *101*, 8914.
(56) Hori, H.; Sarto, J.; Yonetani, T. *J. Biol. Chem.* **1981**, *256*, 7849−7855.
(57) Tyryshkin, A. M.; Dikanov, S. A.; Reijerse, E. J.; Burgard, C.; Hüttermann, J. *J. Am. Chem. Soc.* **1999**, *121*, 3396−3406. (b) Kappe, R.; Hüttermann, J. In *Advanced EPR Applications in Biology and Biochemistry*; Hoff, A. J., Ed.; Elsevier: Amsterdam, 1989.
(58) Ileperuma, O. A.; Feltham, R. D. *Inorg. Chem.* **1977**, *16*, 1876.

cally coupled to an NO^- ($S = 1$) or high-spin Fe^{III} ($S = {}^5/_2$) antiferromagnetically coupled to an NO^- ($S = 1$)) and Fe^{IV} ($S = 1$) antiferromagnetically coupled to NO^- ($S = 1$). For *trans*-[(cyclam)Fe(NO)Cl]^0, an {Fe−NO}^{8} ($S = 0$) species, we arrive at the conclusion that a low-spin ferric ion ($S = {}^1/_2$) is antiferromagnetically coupled to an NO^{2-} ($S = {}^1/_2$) ion. Our results are in excellent agreement with those of Solomon et al. for all {Fe−NO}^{7} ($S = {}^3/_2$) species where the high-spin ferric ($S = {}^5/_2$) electron configuration has been independently established by Fe K-edge XAS, magnetic circular dichroism, resonance Raman, EPR, and Mössbauer spectroscopy.[7,12]

Acknowledgment. We thank the Fonds der Chemischen Industrie for financial support. B. Mienert is thanked for measuring many Mössbauer spectra. We are grateful to Dr. Karsten Meyer for many helpful suggestions concerning the syntheses.

Supporting Information Available: Tables of crystallographic and structure refinement data, atom coordinates, bond lengths and angles, anisotropic thermal parameters, and calculated positional parameters of H atoms for complexes **1** and [L′Fe(NO)(ONO)(NO_2)](ClO_4) (PDF) and an X-ray crystallographic file in CIF format. Figures S1, S2, S3, and S4 displaying variable-temperature, variable-field magnetization curves of [LFe(NO)(N_3)$_2$]; variable-temperature zero-field Mössbauer spectra of [LFe(NO)(N_3)$_2$], **2**, [L′Fe(NO)(ONO)(NO_2)](ClO_4), [Fe^{II}($P(OC_2H_5)_3$)$_5$Br](ClO_4), and [Fe(NO)($P(OC_2H_5)_3$)$_4$]BPh_4, and applied field Mössbauer spectra at 4.2 K of *trans*-[(cyclam)(NO)(Cl)]$^{2+}$ and [L′Fe(NO)(ONO)(NO_2)](ClO_4) (PDF). This material is available free of charge via the Internet at http://pubs.acs.org.

JA994161I